HHS Public Access

Author manuscript

Cell Rep. Author manuscript; available in PMC 2025 June 16.

Published in final edited form as:

Cell Rep. 2025 May 27; 44(5): 115704. doi:10.1016/j.celrep.2025.115704.

Adipocyte metabolic state regulates glial phagocytic function

Mroj Alassaf[1,3], **Aditi Madan**[1,3], **Sunidhi Ranganathan**[1], **Shannon Marschall**[1], **Jordan J. Wong**[1], **Zachary H. Goldberg**[1], **Ava E. Brent**[1,2], **Akhila Rajan**[1,4,*]

[1]Basic Sciences Division, Fred Hutchinson Cancer Center, Seattle, WA 98109, USA

[2]Present address: Department of Biological Sciences, Columbia University, New York, NY, USA

[3]These authors contributed equally

[4]Lead contact

SUMMARY

Excess dietary sugar profoundly impacts organismal metabolism and health, yet it remains unclear how metabolic adaptations in adipose tissue influence other organs, including the brain. Here, we show that a high-sugar diet (HSD) in *Drosophila* reduces adipocyte glycolysis and mitochondrial pyruvate uptake, shifting metabolism toward fatty acid oxidation and ketogenesis. These metabolic changes trigger mitochondrial oxidation and elevate antioxidant responses. Adipocyte-specific manipulations of glycolysis, lipid metabolism, or mitochondrial dynamics non-autonomously modulate Draper expression in brain ensheathing glia, key cells responsible for neuronal debris clearance. Adipocyte-derived ApoB-containing lipoproteins maintain basal Draper levels in glia via LpR1, critical for effective glial phagocytic activity. Accordingly, reducing ApoB or LpR1 impairs glial clearance of degenerating neuronal debris after injury. Collectively, our findings demonstrate that dietary sugar-induced shifts in adipocyte metabolism substantially influence brain health by modulating glial phagocytosis, identifying adipocyte-derived ApoB lipoproteins as essential systemic mediators linking metabolic state with neuroprotective functions.

In brief

An obesogenic diet alters lipid metabolism in *Drosophila* adipocytes, remotely disrupting glial phagocytic function. Alassaf et al. identify adipocyte-derived ApoB and receptor LpR1 as crucial regulators of glial Draper expression and neuronal debris clearance, establishing a link between peripheral lipid metabolism and neuroprotection.

Graphical Abstract

*Correspondence: akhila@fredhutch.org.

AUTHOR CONTRIBUTIONS

Conceptualization, M.A., A.M., and A.R.; methodology and experimentation, M.A., A.M., A.R., S.R., S.M., A.E.B., and Z.H.G.; formal analysis, A.M., M.A., S.M., S.R., J.J.W., and Z.H.G.; writing – original draft, A.R. and M.A.; revision, review, editing, and finalization of the manuscript, A.R. and A.M.; funding acquisition, supervision, and project administration, A.R.

DECLARATION OF INTERESTS

The authors declare no competing interests.

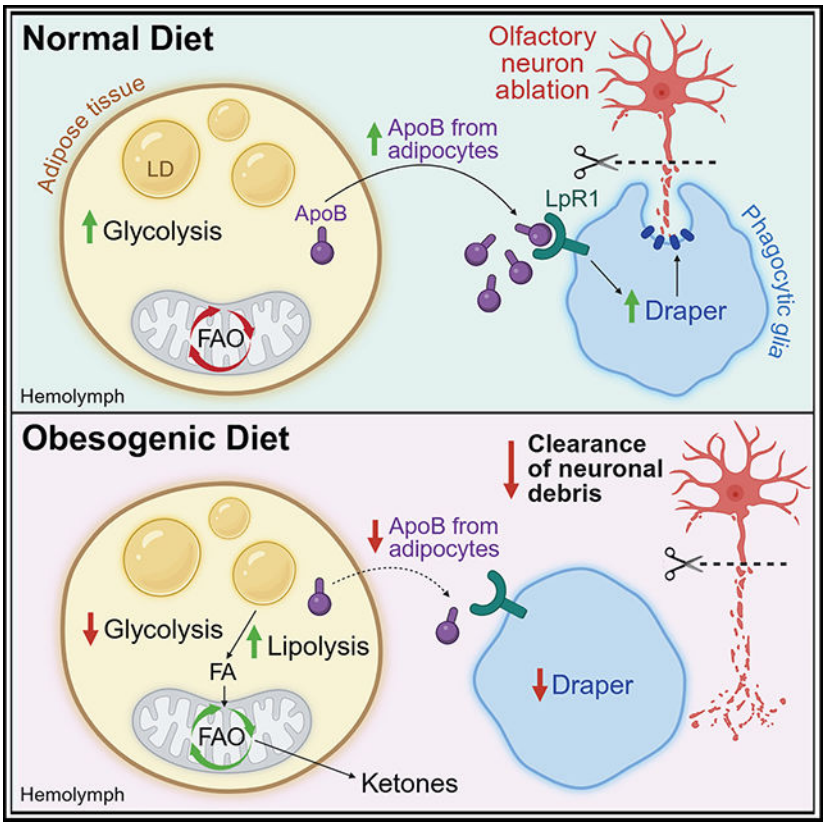

INTRODUCTION

Obesity and type 2 diabetes significantly increase the risk for dementia and neurodegenerative diseases.[1–4] Although mechanisms linking metabolic disorders to cognitive decline remain incompletely defined, disruption of the adipose tissue-brain axis is strongly implicated.[5–8] Once considered merely an energy storage depot, adipose tissue is now recognized as a dynamic endocrine organ secreting diverse molecules that influence brain function, including lipid metabolites and adipokines.[9] These adipocyte-derived factors modulate neuroinflammation, oxidative stress, and synaptic plasticity.[6,8,10] Thus, uncovering mechanisms of adipose-brain communication holds promise for therapeutic strategies against neurodegeneration.

Although the majority of brain lipids are synthesized locally,[11] a fraction is derived from peripheral tissues, especially adipose stores.[12–14] Lipoproteins facilitate inter-organ lipid transport, primarily through apolipoproteins acting as lipid chaperones. Apolipoprotein B (ApoB) delivers peripheral lipids into the brain by binding to low-density lipoprotein receptors (LDLRs) at the blood-brain barrier.[15–18] Dysfunctional ApoB signaling is linked to obesity, diabetes,[19–21] and neurodegeneration[22,23]; however, direct causative roles remain unexplored.

Lipoproteins, composed of apolipoproteins surrounding a lipid core, facilitate lipid transport between tissues. In *Drosophila*, lipid transport relies on lipophorins (Lpp), scaffolded by

apolipophorins structurally analogous to mammalian apolipoproteins[24,25]. The fly ApoB ortholog, Apolpp, is processed in adipocytes into two major lipoproteins—ApoLI and ApoLII (collectively ApoB-Lpp)—which primarily circulate diacylglycerol (DAG) and phosphatidylethanolamine (PE).[24–27] ApoB-Lpp is essential for lipid delivery to peripheral tissues and developing organs, similar to mammalian ApoB's role in systemic lipid distribution.[28]

Despite the presence of a restrictive blood-brain barrier, the *Drosophila* brain acquires lipids from circulating ApoB-Lpp.[29] Loss of adipocyte ApoB dramatically reduces brain lipid stores, notably triacylglycerol, underscoring the critical role of ApoB-Lpp in brain lipid supply.[30] ApoB-Lpp delivers lipids through LDL receptor homologs, LpR1 and LpR2, which mediate lipoprotein internalization analogous to mammalian LDLR.[28,31–33]

Within the brain, neuron-glia lipid trafficking is mediated by ApoD/ApoE homologs, Glaz and Nlaz.[34–36] Overexpression of Glaz confers neuroprotection by enabling glial lipid accumulation and reducing oxidative damage.[36,37] Similarly, in humans, the neuroprotective function of ApoE depends on its lipid-handling capacity, with ApoE4 impairing and ApoE2 enhancing glial lipid storage. [35,38] While ApoB-Lpp signaling influences systemic insulin signaling and feeding behavior,[39–41] its role in regulating glial function and neuroprotection remains unknown.

Neurodegenerative disorders are characterized by the accumulation of toxic protein aggregates and cellular debris, leading to neuronal damage and death.[42] Brain-resident phagocytes, microglia, protect neuronal integrity by efficiently clearing debris.[43] In *Drosophila*, ensheathing glia fulfill similar roles, clearing degenerating neuronal material via the conserved engulfment receptor Draper, homologous to mammalian MEGF10.[44–46] Draper-mediated signaling enables glial cells to detect, engulf, and degrade neuronal debris, maintaining neuronal health.[44,47–52] Indeed, in *Drosophila* Alzheimer's disease models, ensheathing glia clear human β-amyloid aggregates through Draper,[53] analogous to microglial function in mammals.[54] However, age and metabolic stress impair glial phagocytic capacity, contributing to neuronal vulnerability.[50,55]

Previously, we have demonstrated that a high-sugar diet (HSD) impairs Draper signaling and glial phagocytosis by inducing glial insulin resistance.[55] Given evolutionary conservation in adipocyte-brain signaling[56,57] and glial biology,[47,58] we hypothesized that the adipocyte metabolic state influences glial function via lipid-based signals, specifically focusing on adipocyte-derived ApoB lipophorins as potential mediators.

Here, we identify a novel adipocyte-glial metabolic coupling linking dietary sugar exposure to impaired glial phagocytic function, potentially underlying the elevated neurodegeneration risk observed with obesity. We show that a prolonged HSD induces shifts in adipocyte lipolysis, mitochondrial dynamics, metabolism, and antioxidant responses, remotely influencing Draper-mediated glial phagocytosis. Specifically, we propose two mechanisms through which adipocyte dysfunction impacts glial biology. First, altered adipocyte mitochondrial metabolism and increased ketogenesis disrupt glial Draper expression. Second, adipocyte-derived ApoB lipoproteins are critical for the glial response to neuronal

injury. Together, these data uncover how the adipocyte metabolic state remotely modulates glial phagocytic capacity, highlighting potential pathways by which peripheral adipose dysfunction contributes to neurodegeneration risk.

RESULTS

Prolonged exposure to an HSD shifts adipocyte metabolism toward mitochondrial oxidative phosphorylation

Cellular energy production balances two major pathways: glycolysis and oxidative phosphorylation (OxPhos).[59] We examined HSD effects in adult *Drosophila* adipocytes by assessing glycolytic enzyme expression. qPCR analysis from abdominal segments of flies on a normal diet (ND) or HSD for 3 weeks showed significant downregulation of HexA and PyK, essential enzymes for glycolytic flux (Figures 1A and 1B). HexA converts glucose to glucose-6-phosphate, while PyK converts phosphoenolpyruvate to pyruvate,[60,61] consistent with reduced glycolytic activity in adipose tissue under a prolonged HSD.

Using a GFP-tagged lactate dehydrogenase (Ldh) reporter, we monitored glycolytic activity.[62] Confocal imaging revealed a marked reduction in Ldh-GFP levels after HSD feeding (Figures 1C and 1D), with decline detectable at 2 weeks (Figure S1). Glycolysis in the brain remains unchanged at this time point,[55] suggesting that adipose tissue is more sensitive to HSD-induced metabolic shifts.

We examined whether reduced glycolytic activity coincides with mitochondrial morphology changes (Figure 1E). Transmission electron microscopy (TEM) of adipose tissue showed that HSD exposure increases lipid droplet size[40] and results in elongated, irregularly shaped mitochondria (Figure 1F). Using mitochondrion-targeted GFP (*mitoGFP*) under the adipocyte-specific Lpp promoter, we found a shift toward elongated mitochondria in HSD-fed flies (Figures 1G, 1G′, and 1H). This correlated with downregulation of the fission gene fis1 and upregulation of the fusion gene opa1, suggesting adaptive remodeling of mitochondrial networks under an HSD (Figure 1I).

Elongated mitochondria have greater OxPhos capacity compared to circular counterparts.[63,64] We assessed the expression of key OxPhos genes and mitochondrial substrate carriers (Figure 1J). CoxIV, a crucial complex IV component required for mitochondrial respiration, was significantly elevated in adipose tissue following an HSD (Figure 1K). Mitochondrial pyruvate carriers (MPC1 and MPC2) showed marked upregulation, consistent with enhanced mitochondrial pyruvate transport under an HSD (Figure 1K).

To directly assess mitochondrial metabolic activity, we employed genetically encoded mito-Pyronic sensors,[65] in which a circularly permuted GFP (cpGFP) fused to the bacterial PdhR transcription factor, which binds pyruvate. Pyruvate binding causes a fluorescence intensity shift that enables real-time tracking of mitochondrial pyruvate uptake[65] (Figure 1G). The *mitoPyronicSF* sensor measures mitochondrial pyruvate concentration, transport, and flux in real time through a cpGFP fused to the bacterial PdhR transcription factor.[65] Using the *Lpp* promoter to express *mitoPyronicSF* in fat tissue, we found significantly

increased mitochondrial pyruvate uptake in HSD-fed flies at baseline compared to ND-fed flies (Figure 1L). Upon adding 5 mM pyruvate, mitochondrial activity increased in both groups; however, while ND flies exhibited a plateau between 5 and 10 mM pyruvate, HSD-fed flies showed a sustained significant increase in sensor activity (Figures 1L and 1L′), suggesting that HSD-fed mitochondria retain elevated capacity for pyruvate uptake or utilization.

Our findings indicate that HSD enhances mitochondrial pyruvate uptake and activity, supporting a shift toward mitochondrial metabolic activity under HSD stress. Collectively, adipose tissue undergoes a metabolic shift toward increased mitochondrial activity following prolonged HSD exposure, evidenced by decreased glycolysis, altered mitochondrial morphology, upregulation of OxPhos-related genes, and enhanced mitochondrial engagement in response to substrate availability.

HSD shifts adipose metabolism toward fatty acid oxidation and ketogenesis

In obesity and type 2 diabetes, chronic hyperinsulinemia induces insulin resistance, disrupting lipid homeostasis and increasing lipolysis and fatty acid oxidation (FAO).[66,67] FAO generates acetyl-coenzyme A (CoA), which fuels the mitochondrial TCA cycle to support OxPhos.[68] Given that HSD reduces glycolysis (Figures 1B–1D) and increased mitochondrial activity in fly adipose tissue (Figure 1L), we hypothesized a compensatory increase in FAO (see the schematic in Figure 2A).

Perilipin 1 (Plin1/Lsd1 in flies[69,70]) restricts lipolysis.[71–73] Immunohistochemistry showed reduced Plin1 levels in HSD-fed flies, consistent with increased lipolysis (Figures 2B and 2C). qPCR revealed upregulation of hepatocyte nuclear factor 4 (*hnf4*), a regulator of lipid mobilization and FAO, and carnitine palmitoyltransferase 1 (*CPT1A*/*whd* in flies[74]), which facilitates mitochondrial fatty acid transport (Figure 2D). HSD downregulated acyl-coA carboxylase (ACC), potentially enhancing mitochondrial fatty acid uptake. Mitochondrial FAO enzymes, including acetoacetyl-CoA thiolase (*Acat1*), were upregulated (Figure 2E), supporting a shift toward FAO.

Acat1 catalyzes the first step of ketogenesis.[75] Metabolite profiling confirmed increased acetylcarnitine in HSD-fed flies (Figure 2F), reflecting increased acetyl-CoA availability during active FAO.[76,77] We observed increased succinylcarnitine, succinate, and NAD^+—metabolites that feed into the TCA cycle and OxPhos[78] (Figure S2). Acetylcarnitine serves as an acetyl donor for ketogenesis, with levels rising during increased FAO.[79] Metabolomics analysis detected increased α-hydroxybutyrate (α-HB) and β-hydroxybutyrate(β-HB) in whole flies after 2 weeks of HSD feeding (Figure 2G) and in the circulation after 1 week (Figure S2). These findings suggest that HSD promotes FAO and ketone body accumulation in adipose tissue.

Since FAO-driven OxPhos generates ROS, we investigated whether HSD-induced mitochondrial expansion was associated with oxidative stress using MitoTimer. [80,81] After 3 weeks on HSD, flies exhibited a lower red-to-green fluorescence ratio, suggesting reduced ROS levels in adipose mitochondria (Figures 2H and 2H’). One explanation is increased antioxidant defenses. β-HB, elevated in HSD-fed flies, enhances antioxidant responses.[82]

qPCR showed increased expression of nuclear factor erythroid 2-related factor 2 (*nrf2*), a regulator of antioxidant pathways (Figure 2I).

These findings demonstrate that an HSD induces a metabolic shift in adipose tissue, favoring FAO and ketogenesis while upregulating antioxidant defenses to mitigate ROS accumulation. This adaptation maintains energy homeostasis under conditions of impaired glycolysis and insulin resistance.

Adipocyte mitochondrial and lipid metabolism remotely impacts the glial phagocytic state

Given the established role of lipid-derived metabolites in systemic metabolic communication,[76,78] we investigated whether HSD-induced changes in adipocyte mitochondrial and lipid metabolism influence glial function. Glial cells rely on lipid metabolism[83] and maintain brain health during metabolic challenges.[84,85] Aging and an HSD reduce microglial efficiency, leading to chronic inflammation.[50,55] *Drosophila* ensheathing glia serve as the brain's resident phagocytes.[48] Central to glial phagocytosis is *Draper*, the *Drosophila* homolog of the MEGF10 family of receptors.[51,86] *Draper* is essential for pruning axons during development[87,88] and responding to axon injury[51] and clearance of degenerating axons.[87] We have shown previously that an HSD impairs ensheathing glial phagocytic function by inducing glial insulin resistance, downregulating *Draper*.[55] We observed that an HSD alters mitochondrial metabolism and disrupts lipid homeostasis in adipose tissue (Figures 1 and 2). Hence, we explored whether HSD-induced changes in adipocyte-glia metabolic signaling contribute to defects in glial phagocytosis.

We examined how genetic modulation of adipocyte metabolic pathways affects *Draper* expression in ensheathing glia surrounding olfactory neuropil in the antennal lobe (Figure 3A, schematic). A representative image of the adult fly brain stained with *Draper* is shown in Figure 3A'. We genetically manipulated key genes involved in lipid metabolism (Figure 3B) and mitochondrial function (Figure 3C) and then assessed the basal glial phagocytic state.

Previously, we have shown that a prolonged HSD reduced fatty acid (FA) levels.[40] Here, we find that a prolonged HSD upregulates FA oxidation in adipose tissue (Figure 2). We investigated whether altered adipocyte FA homeostasis impacts glial phagocytic receptor expression by genetically manipulating FA metabolism in adipocytes (Figure 3B). *Plin1* restricts lipolysis and FA production. We hypothesized that adipocyte-specific alterations in *Plin1* and the lipase *brummer* (*bmm*)[89,90] would alter FA homeostasis and impact glial phagocytic receptor expression. Overexpression of human *Plin1*[70] in *Drosophila* adipocytes led to increased glial *Draper* levels (Figures 3D–3D'), whereas knockdown of *bmm* lipase reduced *Draper* expression (Figures 3E and 3E'). Knocking down *Plin1* decreased *Draper* expression (Figure S3A). We tested *CPT1A*, required for mitochondrial FA uptake.[74] Pharmacological inhibition of *CPT1A* reduced FA levels,[91] and we found that adipocyte-specific knockdown of *CPT1A* reduced FA levels (Figure S3B). *CPT1A* knockdown significantly reduced *Draper* expression in ensheathing glia (Figures 3F and 3F'). In summary, perturbations in FA homeostasis (Figures 3D–3F) in adipocytes alter the basal glial phagocytic state.

Since glia utilize ketone bodies as an alternative energy source,[92] we examined whether ketogenesis influences glial *Draper* expression. β-hydroxybutyrate shifts brain metabolism from glycolysis toward OxPhos.[93] Given that glial activation requires a glycolytic shift,[94,95] we hypothesized that ketone bodies suppress glial activation and reduce *Draper* expression. Supporting this, an HSD induces a shift toward OxPhos at the expense of glycolysis in the brain.[55] To test whether adipocyte-derived ketone bodies regulate *Draper* expression, we knocked down *Acat1*, a key enzyme in ketogenesis. Suppressing ketone body production significantly increased *Draper* expression, indicating that adipocyte-derived ketone bodies negatively regulate glial *Draper* levels (Figures 3G and 3G').

To assess whether HSD-induced mitochondrial elongation affects glial *Draper* expression, we knocked down the mitochondrial fission factor *Fis1* in adipose tissue, resulting in reduced glial *Draper* expression (Figures 3H and 3H'). We investigated whether adipocyte reactive oxygen species (ROS) levels influence glial *Draper* signaling. Since HSD-fed flies exhibit reduced mitochondrial oxidation and elevated antioxidant activity (Figures 2H and 2I), we reasoned that increasing adipocyte ROS should enhance *Draper* expression. RNAi-mediated knockdown of the mitochondrial antioxidant *Sod2* in adipocytes led to increased glial *Draper* expression (Figures 3I and 3I'). Conversely, overexpression of *Catalase* reduced *Draper* levels, phenocopying effects in HSD-fed flies (Figures 3J and 3J'). These findings indicate that adipocyte mitochondrial metabolism and redox balance regulate glial *Draper* expression.

Hence, in *Drosophila*, adipocyte lipid metabolism and mitochondrial dynamics exert remote influence over the glial phagocytic state.

Adipocyte-derived ApoB lipoprotein signals regulate glial phagocytic response to neuronal injury

Leptin and its *Drosophila* ortholog, *Upd2*, regulate satiety via JAK/STAT signaling in the brain.[57,96,97] Given JAK/STAT's role in maintaining Draper levels in ensheathing glia during axonal injury,[98] we tested whether *upd2* regulates the glial phagocytic state. However, Draper levels remained unchanged in *upd2Δ* deletion mutants,[99] indicating that adipo-glial coupling occurs through another adipocyte-derived signal (Figure S4).

Adipose tissue distributes lipids to multiple organs via ApoB lipoproteins (ApoB-Lpps). *Drosophila* ApoB undergoes post-translational cleavage, producing ApoLI and ApoLII.[27,30,39] ApoLII contains the lipid-binding domain,[27] for which we have previously generated and validated reagents.[40] For clarity, hereafter we refer to ApoLII as ApoB.

An HSD reduces ApoB delivery to the brain, confirmed by western blot analysis of adult fly brains showing decreased endogenous ApoB levels compared to ND controls (Figure 4A). Previous studies have shown that ApoB primarily delivers PE-rich lipids to the brain.[27] Consistently, hemolymph lipid analysis showed a decrease in PE-rich phospholipids, the major component of *Drosophila* lipophorins[27] (Figure S5; Tables S1 and S2), supporting reduced ApoB-mediated lipid transport. Under ND conditions, ApoB localized to glial regions expressing Draper, while an HSD significantly reduced this co-localization (Figures 4B–4B'), suggesting impaired ApoB signaling in glia.

We hypothesized that reduced glial Draper under an HSD resulted from diminished ApoB signaling. Adipocyte-specific ApoB knockdown significantly reduced basal Draper expression (Figures 4C and 4C'). Following antennal ablation,[51] Draper upregulation occurred in controls but failed in ApoB-RNAi flies (Figure 4D), mirroring HSD effects. These results establish that adipocyte-derived ApoB supports both basal and injury-induced Draper expression. Significantly, adipocyte-derived ApoB knockdown did not affect *Drosophila* insulin-like peptide 5 levels (Figure S6), suggesting that ApoB regulation occurs independent of insulin signaling.

The LDLRs LpR1 and LpR2[28] facilitate ApoB-chaperoned lipid uptake. Ensheathing glia-specific knockdown of these receptors non-significantly reduced basal Draper levels (Figures 4E and 4E'). However, post-injury Draper upregulation failed in both *LpR1*- and *LpR2*-RNAi flies (Figure 4F), phenocopying adipocyte-specific ApoB knockdown. This suggests that ApoB-chaperoned lipophorins maintain glial phagocytic competency post injury via LpR1/2 signaling.

To assess functional consequences, we knocked down these receptors in ensheathing glia expressing membrane-tagged GFP in olfactory neurons. Post antennal ablation (Figure 4G), *LpR1* knockdown significantly impaired phagocytosis, shown by increased GFP retention (Figures 4H and 4H'). Surprisingly, LpR2 knockdown did not significantly impact debris clearance despite similar effects on Draper signaling. This suggests that downstream Draper pathways are specifically disrupted in *LpR1* knockdowns but may be unaffected or compensated for in *LpR2* knockdowns (discussion). These findings establish that adipocyte-to-glia *LpR1*-mediated ApoB signaling supports glial phagocytic function by regulating Draper expression post injury.

Collectively, our results reveal a previously unrecognized role of adipose tissue in maintaining glial phagocytic function via lipoprotein-mediated signaling. Importantly, we demonstrate that a prolonged HSD disrupts adipo-glial coupling, impairing glial debris clearance.

DISCUSSION

The adipose tissue-brain axis controls glial response to neuronal injury

The adipose-brain axis is increasingly recognized for its role in brain health, with adipocytes secreting diverse signals influencing brain function. Our study demonstrates that dietary sugar-induced obesity disrupts adipocyte lipid homeostasis, impairing glial phagocytic activity via a novel metabolic coupling involving adipocyte-derived ApoB lipoproteins and glial LpR1.

Recent mammalian studies highlight adipocyte-derived leptin influencing glial metabolism during peripheral nerve injury.[100] However, our findings suggest that adipocyte-glia metabolic coupling in *Drosophila* does not depend on the leptin homolog Upd2 but, rather, involves ApoB-Lpp signaling. This highlights the complexity of adipocyte-glia interactions, indicating distinct signaling pathways regulating different glial populations. Importantly, our

work reveals that adipocyte-derived signals extend beyond traditional adipokines to include lipid-based signaling via ApoB lipoproteins.

Starvation amid nutritional abundance: Adipocyte metabolic adaptation in diet-induced insulin resistance

During starvation, adipocytes adapt by enhancing lipolysis, releasing FAs to provide alternative energy sources and increasing FAO to compensate for reduced glycolysis. Remarkably, metabolic changes observed in insulin resistance resemble the body's response to starvation.[101] Consistent with this, we found that prolonged exposure to an HSD reduces adipocyte glycolytic enzymes (HexA, PyK, and Ldh) while simultaneously increasing key FAO enzymes. These adaptations may initially sustain energy homeostasis, but chronic FAO dependence can elevate lipid metabolites, potentially causing lipotoxic effects in distant tissues, including the brain.[102,103] Indeed, a prolonged HSD increased ketone bodies, typically elevated during nutrient scarcity, supporting the concept that prolonged sugar intake paradoxically induces starvation-like metabolic responses in adipocytes.

A prolonged HSD alters mitochondrial dynamics in adult adipocytes

We observed that HSD-induced mitochondrial elongation and antioxidant upregulation in adipocytes remotely regulate glial Draper levels. Elongated mitochondria generally enhance OxPhos efficiency[63,64] and reduce ROS; however, the exact signaling from mitochondria to glia remains unclear. Potential mechanisms include antioxidant-induced shifts in adipocyte-secreted metabolites that modulate glial Draper signaling. Additionally, reduced mitochondrial oxidation in adipocytes after a prolonged HSD, driven by increased Nrf2-mediated antioxidant responses, may represent a hormetic adaptation, initially triggered by transient oxidative stress. This response mirrors observations in mouse heart tissue under obesogenic stress.[104] Another plausible explanation for enhanced antioxidant defense includes increased adipose lipid droplet storage, which buffers ROS accumulation.[105,106]

Moreover, heightened FAO typically enhances mitochondrion-lipid droplet interactions, efficiently transferring FAs into mitochondria and preventing cytosolic oxidation, thereby reducing oxidative stress.[107,108] Although adipocyte glycolysis declines during HSD feeding, elevated mitochondrial pyruvate uptake suggests alternative pyruvate sources, potentially from amino acid catabolism, glycerol metabolism, or TCA cycle intermediates replenished via FAO.[76] Future investigations of these metabolic shifts will provide deeper insights into adipocyte metabolic adaptation under chronic dietary sugar stress.

ApoB-Lpp signals through glial LpR1 to regulate Draper expression and phagocytosis

Our findings establish ApoB-Lpp as critical systemic regulators of glial Draper expression and phagocytic function. ApoB-Lpp are known to deliver lipids to peripheral tissues through LDL receptor-mediated internalization.[28] The knockdown of LDLR homologs *LpR1* or *LpR2* individually did not alter basal Draper levels but impaired injury-induced Draper upregulation, suggesting redundancy in maintaining basal Draper expression but critical roles during injury responses. Interestingly, *LpR1* knockdown impaired glial phagocytosis of neuronal debris after injury, whereas *LpR2* knockdown had no such effect. Similar context-specific receptor roles occur during lipoprotein delivery to ovaries,[28] supporting

the idea that LpR1 may specifically mediate injury-induced glial responses. Indeed, activity-dependent LpR1 upregulation influences dendritic morphogenesis in larvae,[109] raising the possibility that neuronal injury similarly induces LpR1, enhancing Draper expression and phagocytic capacity. Future studies should clarify how ApoB-LpR1 signaling precisely regulates Draper-mediated phagocytosis.

ApoB primarily transports PE-rich lipids,[27] which directly bind Draper.[110] In our prior work, we have shown that prolonged HSD exposure reduces PE levels in whole-fly lysates,[40] and in this study, we showed that circulating PE levels are also impacted. Draper, a multi-liganded receptor, binds PE-rich lipid membranes through its EMI and NIM domains, possibly activating an auto-regulatory feedback loop that maintains basal phagocytic activity.[98,110–112] Thus, reduced PE-lipid availability under an HSD could directly impair basal Draper levels independent of LpR signaling. Recent studies also suggest that systemic lipid signals, especially ApoB, regulate phagocytic receptor expression in *Drosophila* immune cells.[113] Thus, ApoB-Lpp-mediated lipid signaling could represent a conserved mechanism regulating phagocytic competence across cell types.

In conclusion, our findings reveal direct communication from adipocyte lipid metabolism and mitochondrial state to glial phagocytic function via ApoB lipoproteins. Given clinical correlations linking obesity and cognitive decline,[1–4] this work provides critical insight into how dysfunctional adipocyte metabolism can impact brain health.

Limitations of the study

While our study provides strong evidence linking adipocyte mitochondrial metabolism and ApoB-LpR1 signaling to glial phagocytic function, several limitations should be considered. First, although *Drosophila* is a powerful genetic model with conserved metabolic pathways, translation of these findings to mammalian systems, particularly humans, requires further validation. Second, the precise molecular identities of lipid metabolites and reactive intermediates responsible for remote signaling between adipocytes and glia remain unclear. The proposed mediators (PE-rich lipids and ketone bodies) require explicit validation in future *in vivo* studies. Finally, while our findings demonstrate correlations between mitochondrial morphology and glial signaling, additional work is necessary to pinpoint specific factors that communicate the adipocyte mitochondrial metabolic state to the brain, particularly under obesogenic stress conditions.

RESOURCE AVAILABILITY

Lead contact

Requests for further information and resources should be directed to and will be fulfilled by the lead contact, Akhila Rajan (akhila@fredhutch.org).

Materials availability

All reagents generated in this study are available from the lead contact without restriction.

Data and code availability

- This paper does not report original code.
- All data generated or analyzed during this study are included in this published article and its supplemental information. The source data underlying the metabolite profiling has been deposited in the General Data Repository Fig Share. The links to the public datasets are provided in the key resources table.
- Any additional information required to reanalyze the data reported in this paper is available from the lead contact upon request.

STAR★METHODS

EXPERIMENTAL MODEL AND STUDY PARTICIPANT DETAILS

***Drosophila melanogaster* strains and husbandry:** The *Drosophila* strains used in this study are listed in the key resources table. Flies were housed at 25°C, and experiments utilized 7–10-day-old adult male flies. The flies' diet consisted of 15 g yeast, 8.6 g soy flour, 63 g corn flour, 5 g agar, 5 g malt, and 74 mL corn syrup per liter. Diet formulations were normal diet (ND) or high sugar diet (HSD) with added sucrose (300 g/L).

METHOD DETAILS

Antennal nerve injury: As adapted from prior studies by Freeman & Logan et al.,[44,51,52,116–118] Briefly, flies were anesthetized using CO_2, and antennal nerve injury was accomplished by unilaterally removing the third antennal segment using forceps. Flies were then placed back into the vial post-injury until dissection 24 h later.

Immunostaining: Adult brains and fat bodies were dissected in ice-cold PBS, fixed overnight in 0.8% paraformaldehyde (PFA) in PBS at 4°C. Fixed brains were washed 5 times in PBS with 0.5% BSA and 0.5% Triton X-100 (PAT), blocked for 1 h in PAT +5% NDS, incubated overnight with primary antibodies, followed by 5 washes with PAT, re-blocking for 30 min, and secondary antibody incubation for 2–4 h at RT. Finally, the brains were washed 3 times in PAT and mounted using Slow fade gold antifade.

Image analysis: Images were acquired with a Zeiss LSM 800 and Leica Stellaris confocal system. Images were analyzed using ImageJ. All images within each experiment were acquired with the same confocal settings. z stack summation projections at 0.5 μm intervals were generated, and a region of interest (indicated in the fig) was used to measure the integrated density values of each fluorescent tag. A maximum-intensity projection of Z-stacks that covered the full depth of the antennal lobe was used for ImageJ analysis to measure mitochondrial morphology.

To measure the average mitochondrial circularity major and minor axes, we adapted methods from prior work.[119] Maximum-intensity projection was inverted and automatic threshold completed before applying the 'analyze particles' function to measure the average mitochondrial circularity. Mitochondrial elongation (Aspect ratio) was measured from the same maximum intensity projection using the ImageJ plugin developed by work from

Chaudry et al.,[119] The size and dimensions of all ROIs were maintained consistently throughout each experiment.

Dilp5 levels were quantified using z stack summation projections to capture the full depth of the IPCs. A region of interest (ROI) around the IPCs was manually outlined with the freehand tool, and integrated density values were then measured.

For co-localization analysis, confocal images were acquired using Zeiss LSM 800 with a 63× oil immersion objective at 2X zoom. Co-localization analysis was performed using Mander's overlap coefficient (MOC) to quantify the degree of signal overlap between ApoB and Draper. One measurement per z-slice for each image ($N = 11$) was performed, to ensure that the measurement is not affected by tissue depth and the resulting change in intensity.

MitoPyronic sensor live imaging: The pyruvate sensor expressing fly stock UAS-*MitoPyronicSF* were procured from BDSC (Stock #94536). Flies expressing the sensor in adult fat were aged for 3 weeks on either normal diet (ND) or high sugar diet (HSD) at 25°C. *Drosophila* abdomens were dissected in HL3 buffer (70mM NaCl, 5mM KCl, 20mM $MgCl_2$, 10mM $NaHCO_3$, 115mM sucrose, 5mM trehalose, 5mM HEPES; pH 7.1), and mounted on a glass-bottom FluoroDish (WPI, Cat#FD3510–100). Image stacks were acquired with a Zeiss LSM 800 using a 20X air lens (Plan-Apochromat 20x/0.8) at 0.5μm intervals. Pyruvate (Agilent, Cat#103578–100) was superfused manually from the side, such that the dissected tissue was not disturbed. Imaging was done within 60 s of addition of each concentration of pyruvate. GFP signal intensity in the acquired images was measured using ImageJ.

Transmission electron microscopy (TEM): Adipocyte explants were prepared for transmission electron microscopy (TEM) by fixation in a solution containing 1.25% formaldehyde, 2.5% glutaraldehyde, and 0.03% picric acid in 0.1M cacodylate buffer (pH 7.4). Following fixation, the samples were stained with osmium tetroxide and uranyl acetate, then progressively dehydrated through a graded ethanol series and propylene oxide. For embedding, the samples were infiltrated with a 1:1 mixture of EPON resin (Westlake) and propylene oxide at 4°C for 16 h before polymerization in pure EPON resin at 60°C for 24 h. The embedded samples were sectioned using standard ultramicrotomy techniques and examined with a JEOL 1200EX transmission electron microscope.

Quantitative PCR (qPCR): Thirty flies were dissected in RNAlater, then placed in 30 μL of TriReagent and a scoop of beads in a 1.5 mL safelock tube. The abdominal segments dissected from flies were homogenized using a bullet blender. RNA was then isolated using a Direct-zol RNA microprep kit following the manufacturer's instructions. Isolated RNA was synthesized into cDNA using the Bio-Rad iScript RT supermix for RT-qPCR, and qPCR was performed using the Bio-Rad ssoAdvanced SYBR green master mix. Primers were designed using DRSC's FlyPrimer Bank[120] and are listed in Table S3. Relative mRNA quantification was performed using the comparative CT method and normalized to alpha-tubulin mRNA expression. Three technical replicates were used for each gene.

Western blotting: 10–12 flies were homogenized in triplicates using 1mm zirconium beads (Cat#ZROB10, Next Advance) in a Bullet Blender Tissue homogenizer (Model BBX24, Next Advance) in 250 μL of a mixture containing 200 μL of diH2O and 2 μL of HALT Protease Inhibitor Cocktail (ThermoFisher, Cat#87786), along with 50 μL of 5x RIPA Buffer (ThermoFisher, Cat# J62524.AD) in 1.5 mL LoBind Eppendorf Tubes (Eppendorf, Cat#022431081). Samples were incubated on a rocking platform for 30–60 min at 4°C. Subsequently, the tubes were centrifuged at 10,000 × g at 4°C for 10 min, and the supernatant was carefully collected into separate 1.5 mL tubes. Protein quantification was performed on all three lysate samples using the Pierce BCA Protein Assay Kit (ThermoScientific Cat#23228, Cat#1859078). Samples were then prepared for western blotting by adjusting the concentration to 2 μg/μL using 4x Laemmli Sample Buffer (Bio-Rad Cat#161047) and TCEP Bond Breaker (Thermo Scientific Cat#77720), followed by heating at 95°C for 5–10 min.

For preparing protein lysates from adult *Drosophila* brains, 5 μL of lysis buffer (0.1% SDS in PBS with HALT) was added to a PCR tube. 10 brains were dissected and placed in the lysis buffer. 10 μL of Laemmli buffer was added per tube. Samples were boiled at 95°C for 10 min.

Equal amounts of protein (10 μg per lane for whole fly lysates; 12μL per lane for brain lysates) were loaded onto SDS-PAGE gels (Bio-Rad, Cat#4561103). Precision Plus Protein Dual Color Standards (Bio-Rad, Cat#1610374) were included as molecular weight markers. Following electrophoresis, proteins were transferred from the gel to a nitrocellulose membrane using a wet transfer system. The membrane was blocked in Starting Block Blocking Buffer (Thermo Scientific, Cat#37538) in TBS-T (Tris-buffered saline with 0.1% Tween 20) for 1 h at room temperature with gentle agitation to prevent non-specific binding. Primary antibodies against the target protein and loading control were diluted in blocking buffer and TBS-T; Mouse anti-Draper (1:250; DSHB 8A1 RRID: AB_2618106), Rabbit anti-apo2 (1:2500; generated by the Rajan Lab), Mouse anti-Tubulin (1:4000; Sigma Cat#T5168). and incubated with the membrane overnight at 4°C. Membranes were washed and incubated with HRP (horseradish peroxidase)-conjugated secondary antibodies diluted in blocking buffer and TBS-T for 1 h at room temperature. Protein bands were visualized using an enhanced chemiluminescence (ECL) detection system (Abcam, Cat #AB65623). Images were captured using a chemiluminescence imaging system.

Free fatty acid measurements: We used the colorimetric Free Fatty Acid Assay Kit (Sigma Aldrich, Cat#MAK466) and followed the manufacturer's instructions. Briefly, 8 flies were homogenized in 60μL of 5% iso-propanol and 2% Triton X- solution using a pestle in 1.5 mL LoBind Eppendorf Tubes (Eppendorf, Cat#022431081). Samples were centrifuged at 15,000g for 1 min at room temperature. The supernatant was carefully removed to separate 1.5 mL tubes. Triplicates of 10μL (neat) and 5μL (1:2 dilution, made up to 10μL in diH_2O) were used per well of a clear 96-well plate (Corning, Cat#3585). 90μL of working reagent was added (as per manufacturer's instructions). Plates were incubated at room temperature for 30min. Absorbance (OD) was measured at 570nm in a microplate reader.

Hemolymph extraction: For hemolymph extraction, 30 adult flies were anesthetized on a CO2 pad and punctured in the thorax region with a tungsten needle. The flies were then transferred into a 0.5 mL Eppendorf tube with holes made in the bottom using an 18G needle. This 0.5 mL tube was placed inside a 1.5 mL Eppendorf tube containing 30 μL of PBS and centrifuged at 5000 RPM for 5 min. The samples were then flash-frozen in liquid nitrogen until ready to use.

Metabolomics sample preparation: Aqueous metabolites for targeted LC-MS profiling of whole flies and hemolymph samples were extracted using a protein precipitation method similar to the one described elsewhere[121,122] by the Seattle Northwest Metabolomics Research Center (NW-MRC).

Whole fly Samples: Whole adult male flies were frozen in liquid nitrogen after 7 or 14 days on a normal diet or HSD. Ten flies were used per biological sample, and 3 biological replicates were used for each diet and time point. Samples were first homogenized in 200 μL purified deionized water at 4°C. Then 800 μL of cold methanol containing 124 μM 6C13-glucose and 25.9 μM 2C13-glutamate was added (reference internal standards were added to the samples to monitor sample prep). Afterward, samples were vortexed, stored for 30 min at −20°C, sonicated in an ice bath for 10 min, centrifuged for 15 min at 14,000 rpm and 4°C, and then 600 μL of supernatant was collected from each sample. Lastly, recovered supernatants were dried on a SpeedVac and reconstituted in 0.5 mL of LC-matching solvent containing 17.8 μM 2C13-tyrosine and 39.2 3C13-lactate (reference internal standards were added to the reconstituting solvent to monitor LC-MS performance). Samples were transferred into LC vials and placed into a temperature-controlled autosampler for LC-MS analysis.

Hemolymph Samples: 30 flies were used per biological sample, and 3 biological replicates were used for each diet and timepoint. Samples were thawed at 4°C for 60 min and vortexed for 10 s 50uL of each sample was transferred to a 2 mL Eppendorf tube, and 50 μL of 50%MeOH/50%Water containing 30 stable isotope-labeled internal standards (SILISs) was added. Afterward, 250 μL of cold MeOH containing two additional SILISs was added to each sample. Samples were vortexed, stored for 30 min at −20°C, centrifuged for 15 min at 14,000 rpm and 4°C, and then 250 μL of supernatant was collected from each sample. Lastly, recovered supernatants were dried on a SpeedVac and reconstituted in 0.5 mL of LC-matching solvent containing two more SILISs. 34 SILISs were added to the samples in various sample prep steps to monitor sample prep, assay performance, and determine absolute concentrations for the metabolites that had corresponding SILISs.

Metabolomics: Targeted LC-MS metabolite analysis was performed on a duplex-LC-MS system composed of two Shimadzu UPLC pumps, CTC Analytics PAL HTC-xt temperature-controlled auto-sampler, and AB Sciex 6500+ Triple Quadrupole MS equipped with ESI ionization source. UPLC pumps were connected to the auto-sampler in parallel and could perform two chromatography separations independently from each other. Each sample was injected twice on two identical analytical columns (Waters XBridge BEH Amide XP), where separations were performed in hydrophilic interaction liquid chromatography

(HILIC) mode. While one column was performing separation and MS data acquisition in ESI+ ionization mode, the other column was getting equilibrated for sample injection, chromatography separation, and MS data acquisition in ESI− mode. Each chromatography separation was 18 min (total analysis time per sample was 36 min). MS data acquisition was performed in multiple-reaction-monitoring (MRM) mode. LC-MS system was controlled using AB Sciex Analyst 1.6.3 software. Measured MS peaks were integrated using AB Sciex MultiQuant 3.0.3 software. Up to 158 metabolites (plus 4 spiked standards) were measured across the fly samples study set, and up to 148 metabolites (plus 34 SILISs) were measured in the hemolymph sample set. For the hemolymph set, absolute concentrations of 30 metabolites were determined. In addition to the two study samples, two sets of quality control (QC) samples were used to monitor the assay performance and data reproducibility. One QC [QC(I)] was a pooled human serum sample used to monitor system performance, and the other QC [QC(S)] was pooled study samples. This QC was used to monitor data reproducibility. Each QC sample was injected per every 10 study samples. The median CV for the fly set was 2.8%, while for the blood samples was 11.1%.

Lipidomics: Frozen hemolymph samples from ND and HSD-fed flies were sent to the Northwest Metabolomics Research Center (NW-MRC) for targeted quantitative lipid profiling using the Sciex 5500 Lipidyzer as per methods established by NW-MRC.[123] The materials used include LC-MS grade methanol, dichloromethane, and ammonium acetate, all sourced from Fisher Scientific (Pittsburgh, PA). HPLC grade 1-propanol was obtained from Sigma-Aldrich (Saint Louis, MO). Milli-Q water was produced using an in-house Ultrapure Water System by EMD Millipore (Billerica, MA). The Lipidyzer isotope-labeled internal standards mixture, which contained 54 isotopes from 13 different lipid classes, was acquired from Sciex (Framingham, MA). HCER and LCER were not detected in *Drosophila* hemolymph, so we report 11 different lipid classes.

QUANTIFICATION AND STATISTICAL ANALYSIS

Statistical analysis was performed with GraphPad PRISM (GraphPad Software Incorporated). Data are expressed as the mean ± standard deviation (SD). Data normality was assessed via Shapiro-Wilk tests. Parametric analyses included two-tailed unpaired t-tests with Welch's correction or two-way ANOVA with Holm-Sidak correction. Non-parametric analysis employed Mann-Whitney tests. Statistical significance was defined as $p < 0.05$.

ADDITIONAL RESOURCES

FlyBase (release FB2023_05): https://flybase.org/.

Supplementary Material

Refer to Web version on PubMed Central for supplementary material.

ACKNOWLEDGMENTS

We thank Dr. Jason M. Tennessen for generously donating the *Ldh-GFP* transgenic fly line used in this article. We thank Rajan Lab member Dr. Kevin P. Kelly for critical reading, discussions, and comments on the manuscript. We acknowledge the Northwest Metabolomics Research Center (NW-MRC) at the University of Washington, Seattle, for support with lipidomics and metabolomics and NIH grant 1S10OD021562–01, which purchased an

LC-MS system for collecting targeted metabolic profiling data. Dr. Julien Dubrulle at the Cellular Imaging Shared Resources at the Fred Hutch (RRID:SCR_022609) performed the co-localization analysis. We additionally thank the Harvard Electron Microscopy facility for assisting with TEM images of *Drosophila* abdominal adipocytes. Stocks obtained from the Bloomington Drosophila Stock Center (NIH P40OD018537) were used in this study. The Draper monoclonal antibody, developed by Mary Logan (OHSU), was obtained from the Developmental Studies Hybridoma Bank (DSHB), created by the NICHD of the NIH and maintained at The University of Iowa, Department of Biology. This work was possible due to grants awarded to A.R. from the NIH National Institute of General Medical Sciences (R35GM124593) and the McKnight Foundation Neurobiology Disorders (NBD) Award. A postdoctoral fellowship from the Helen Hay Whitney Foundation supported M.A. This work uses resources and shared equipment supported by the Fred Hutch Cancer Consortium grant (P30 CA015704).

REFERENCES

1. Xu WL, Atti AR, Gatz M, Pedersen NL, Johansson B, and Fratiglioni L (2011). Midlife overweight and obesity increase late-life dementia risk: a population-based twin study. Neurology 76, 1568–1574. 10.1212/WNL.0b013e3182190d09. [PubMed: 21536637]
2. Hassing LB, Dahl AK, Thorvaldsson V, Berg S, Gatz M, Pedersen NL, and Johansson B (2009). Overweight in midlife and risk of dementia: a 40-year follow-up study. Int. J. Obes. 33, 893–898. 10.1038/ijo.2009.104.
3. Allen AN, Clarke R, Shipley M, and Leon DA (2019). Adiposity in middle and old age and risk of death from dementia: 40-year follow-up of 19,000 men in the Whitehall study. Age Ageing 48, 247–253. 10.1093/ageing/afy182. [PubMed: 30624572]
4. Verdile G, Fuller SJ, and Martins RN (2015). The role of type 2 diabetes in neurodegeneration. Neurobiol. Dis. 84, 22–38. 10.1016/j.nbd.2015.04.008. [PubMed: 25926349]
5. Kim S, Yi HA, Won KS, Lee JS, and Kim HW (2022). Association between Visceral Adipose Tissue Metabolism and Alzheimer's Disease Pathology. Metabolites 12, 258. 10.3390/metabo12030258. [PubMed: 35323701]
6. Sripetchwandee J, Chattipakorn N, and Chattipakorn SC (2018). Links Between Obesity-Induced Brain Insulin Resistance, Brain Mitochondrial Dysfunction, and Dementia. Front. Endocrinol. 9, 496. 10.3389/fendo.2018.00496.
7. Luchsinger JA, and Gustafson DR (2009). Adiposity and Alzheimer's disease. Curr. Opin. Clin. Nutr. Metab. Care 12, 15–21. 10.1097/MCO.0b013e32831c8c71. [PubMed: 19057182]
8. Oliveras-Canellas N, Castells-Nobau A, de la Vega-Correa L, Latorre-Luque J, Motger-Alberti A, Arnoriaga-Rodriguez M, Garre-Olmo J, Zapata-Tona C, Coll-Martinez C, Ramio-Torrenta L, et al. (2023). Adipose tissue coregulates cognitive function. Sci. Adv. 9, eadg4017. 10.1126/sciadv.adg4017. [PubMed: 37566655]
9. Shimizu H, and Mori M (2005). The brain-adipose axis: a review of involvement of molecules. Nutr. Neurosci. 8, 7–20. 10.1080/10284150500047245. [PubMed: 15909763]
10. Schmitt LO, and Gaspar JM (2023). Obesity-Induced Brain Neuroinflammatory and Mitochondrial Changes. Metabolites 13, 86. 10.3390/metabo13010086. [PubMed: 36677011]
11. Bruce KD, Zsombok A, and Eckel RH (2017). Lipid Processing in the Brain: A Key Regulator of Systemic Metabolism. Front. Endocrinol. 8, 60. 10.3389/fendo.2017.00060.
12. Emma EM, and Amanda J (2022). Dietary lipids from body to brain. Prog. Lipid Res. 85, 101144. 10.1016/j.plipres.2021.101144. [PubMed: 34915080]
13. Pifferi F, Laurent B, and Plourde M (2021). Lipid Transport and Metabolism at the Blood-Brain Interface: Implications in Health and Disease. Front. Physiol. 12, 645646. 10.3389/fphys.2021.645646. [PubMed: 33868013]
14. Rosen ED, and Spiegelman BM (2014). What we talk about when we talk about fat. Cell 156, 20–44. 10.1016/j.cell.2013.12.012. [PubMed: 24439368]
15. Behbodikhah J, Ahmed S, Elyasi A, Kasselman LJ, De Leon J, Glass AD, and Reiss AB (2021). Apolipoprotein B and Cardiovascular Disease: Biomarker and Potential Therapeutic Target. Metabolites 11, 690. 10.3390/metabo11100690. [PubMed: 34677405]
16. Zou Z, Shao S, Zou R, Qi J, Chen L, Zhang H, Shen Q, Yang Y, Ma L, Guo R, et al. (2019). Linking the low-density lipoprotein receptor-binding segment enables the therapeutic 5-YHEDA peptide to cross the blood-brain barrier and scavenge excess iron and radicals in the brain of senescent mice. Alzheimer's Dement. 5, 717–731. 10.1016/j.trci.2019.07.013.

17. Spencer BJ, and Verma IM (2007). Targeted delivery of proteins across the blood-brain barrier. Proc. Natl. Acad. Sci. USA 104, 7594–7599. 10.1073/pnas.0702170104. [PubMed: 17463083]

18. Wang H, and Eckel RH (2014). What are lipoproteins doing in the brain? Trends Endocrinol. Metab. 25, 8–14. 10.1016/j.tem.2013.10.003. [PubMed: 24189266]

19. Onat A, Can G, Hergenç G, Yazici M, Karabulut A, and Albayrak S (2007). Serum apolipoprotein B predicts dyslipidemia, metabolic syndrome and, in women, hypertension and diabetes, independent of markers of central obesity and inflammation. Int. J. Obes. 31, 1119–1125. 10.1038/sj.ijo.0803552.

20. Smith J, Amri MA, and Sniderman AD (2005). What do we (not) know about apoB, type 2 diabetes and obesity? Diabetes Res. Clin. Pract. 69, 99–101. 10.1016/j.diabres.2004.09.012. [PubMed: 15955392]

21. Richardson TG, Wang Q, Sanderson E, Mahajan A, McCarthy MI, Frayling TM, Ala-Korpela M, Sniderman A, Smith GD, and Holmes MV (2021). Effects of apolipoprotein B on lifespan and risks of major diseases including type 2 diabetes: a mendelian randomisation analysis using outcomes in first-degree relatives. Lancet. Healthy Longev. 2, e317–e326. 10.1016/S2666-7568(21)00086-6. [PubMed: 34729547]

22. Picard C, Nilsson N, Labonté A, Auld D, Rosa-Neto P, Ashton NJ, Zetterberg H, Blennow K, and Breitner JCB (2022). Apolipoprotein B is a novel marker for early tau pathology in Alzheimer's disease. Alzheimer's Dement. 18, 875–887. 10.1002/alz.12442. [PubMed: 34590423]

23. Martin L, Boutwell BB, Messerlian C, and Adams CD (2024). Mendelian randomization reveals apolipoprotein B shortens healthspan and possibly increases risk for Alzheimer's disease. Commun. Biol. 7, 230. 10.1038/s42003-024-05887-2. [PubMed: 38402277]

24. Arrese EL, Gazard JL, Flowers MT, Soulages JL, and Wells MA (2001). Diacylglycerol transport in the insect fat body: evidence of involvement of lipid droplets and the cytosolic fraction. J. Lipid Res. 42, 225–234. [PubMed: 11181752]

25. van der Horst DJ, van Hoof D, van Marrewijk WJA, and Rodenburg KW (2002). Alternative lipid mobilization: the insect shuttle system. Mol. Cell. Biochem. 239, 113–119. [PubMed: 12479576]

26. Smolenaars MMW, Madsen O, Rodenburg KW, and Van der Horst DJ (2007). Molecular diversity and evolution of the large lipid transfer protein superfamily. J. Lipid Res. 48, 489–502. 10.1194/jlr.R600028-JLR200. [PubMed: 17148551]

27. Palm W, Sampaio JL, Brankatschk M, Carvalho M, Mahmoud A, Shevchenko A, and Eaton S (2012). Lipoproteins in Drosophila melanogaster–assembly, function, and influence on tissue lipid composition. PLoS Genet. 8, e1002828. 10.1371/journal.pgen.1002828. [PubMed: 22844248]

28. Parra-Peralbo E, and Culi J (2011). Drosophila lipophorin receptors mediate the uptake of neutral lipids in oocytes and imaginal disc cells by an endocytosis-independent mechanism. PLoS Genet. 7, e1001297. 10.1371/journal.pgen.1001297. [PubMed: 21347279]

29. Fernandes VM, Auld V, and Klambt C (2024). Glia as Functional Barriers and Signaling Intermediaries. Cold Spring Harb Perspect Biol 16, a041423. 10.1101/cshperspect.a041423. [PubMed: 38167424]

30. Brankatschk M, and Eaton S (2010). Lipoprotein particles cross the blood-brain barrier in Drosophila. J. Neurosci. 30, 10441–10447. 10.1523/JNEUROSCI.5943-09.2010. [PubMed: 20685986]

31. Herz J, and Bock HH (2002). Lipoprotein receptors in the nervous system. Annu. Rev. Biochem. 71, 405–434. 10.1146/annurev.biochem.71.110601.135342. [PubMed: 12045102]

32. Islam MM, Hlushchenko I, and Pfisterer SG (2022). Low-Density Lipoprotein Internalization, Degradation and Receptor Recycling Along Membrane Contact Sites. Front. Cell Dev. Biol. 10, 826379. 10.3389/fcell.2022.826379. [PubMed: 35141225]

33. Rodriguez-Vazquez M, Vaquero D, Parra-Peralbo E, Mejia-Morales JE, and Culi J (2015). Drosophila Lipophorin Receptors Recruit the Lipoprotein LTP to the Plasma Membrane to Mediate Lipid Uptake. PLoS Genet. 11, e1005356. 10.1371/journal.pgen.1005356. [PubMed: 26121667]

34. Sanchez D, López-Arias B, Torroja L, Canal I, Wang X, Bastiani MJ, and Ganfornina MD (2006). Loss of glial lazarillo, a homolog of apolipoprotein D, reduces lifespan and stress resistance in Drosophila. Curr. Biol. 16, 680–686. 10.1016/j.cub.2006.03.024. [PubMed: 16581513]

35. Yu JT, Tan L, and Hardy J (2014). Apolipoprotein E in Alzheimer's disease: an update. Annu. Rev. Neurosci. 37, 79–100. 10.1146/annurev-neuro-071013-014300. [PubMed: 24821312]
36. Liu L, MacKenzie KR, Putluri N, Maletić-Savatić M, and Bellen HJ (2017). The Glia-Neuron Lactate Shuttle and Elevated ROS Promote Lipid Synthesis in Neurons and Lipid Droplet Accumulation in Glia via APOE/D. Cell Metab. 26, 719–737. 10.1016/j.cmet.2017.08.024. [PubMed: 28965825]
37. Haynes PR, Pyfrom ES, Li Y, Stein C, Cuddapah VA, Jacobs JA, Yue Z, and Sehgal A (2024). A neuron-glia lipid metabolic cycle couples daily sleep to mitochondrial homeostasis. Nat. Neurosci. 27, 666–678. 10.1038/s41593-023-01568-1. [PubMed: 38360946]
38. Genin E, Hannequin D, Wallon D, Sleegers K, Hiltunen M, Combarros O, Bullido MJ, Engelborghs S, De Deyn P, Berr C, et al. (2011). APOE and Alzheimer disease: a major gene with semi-dominant inheritance. Mol. Psychiatry 16, 903–907. 10.1038/mp.2011.52. [PubMed: 21556001]
39. Brankatschk M, Dunst S, Nemetschke L, and Eaton S (2014). Delivery of circulating lipoproteins to specific neurons in the Drosophila brain regulates systemic insulin signaling. Elife 3, e02862. 10.7554/eLife.02862. [PubMed: 25275323]
40. Kelly KP, Alassaf M, Sullivan CE, Brent AE, Goldberg ZH, Poling ME, Dubrulle J, and Rajan A (2022). Fat body phospholipid state dictates hunger-driven feeding behavior. Elife 11, e80282. 10.7554/eLife.80282. [PubMed: 36201241]
41. Ugrankar-Banerjee R, Tran S, Bowerman J, Kovalenko A, Paul B, and Henne WM (2023). The fat body cortical actin network regulates Drosophila inter-organ nutrient trafficking, signaling, and adipose cell size. Elife 12, e81170. 10.7554/eLife.81170. [PubMed: 37144872]
42. Wilson DM, Cookson MR, Van Den Bosch L, Zetterberg H, Holtzman DM, and Dewachter I (2023). Hallmarks of neurodegenerative diseases. Cell 186, 693–714. 10.1016/j.cell.2022.12.032. [PubMed: 36803602]
43. Hickman S, Izzy S, Sen P, Morsett L, and El Khoury J (2018). Microglia in neurodegeneration. Nat. Neurosci. 21, 1359–1369. 10.1038/s41593-018-0242-x. [PubMed: 30258234]
44. Doherty J, Logan MA, Tas,demir OE, and Freeman MR. (2009). Ensheathing glia function as phagocytes in the adult Drosophila brain. J. Neurosci. 29, 4768–4781. 10.1523/JNEUROSCI.5951-08.2009. [PubMed: 19369546]
45. Scheib JL, Sullivan CS, and Carter BD (2012). Jedi-1 and MEGF10 signal engulfment of apoptotic neurons through the tyrosine kinase Syk. J. Neurosci. 32, 13022–13031. 10.1523/JNEUROSCI.6350-11.2012. [PubMed: 22993420]
46. Ziegenfuss JS, Biswas R, Avery MA, Hong K, Sheehan AE, Yeung YG, Stanley ER, and Freeman MR (2008). Draper-dependent glial phagocytic activity is mediated by Src and Syk family kinase signalling. Nature 453, 935–939. 10.1038/nature06901. [PubMed: 18432193]
47. Kremer MC, Jung C, Batelli S, Rubin GM, and Gaul U (2017). The glia of the adult Drosophila nervous system. Glia 65, 606–638. 10.1002/glia.23115. [PubMed: 28133822]
48. Freeman MR (2015). Drosophila Central Nervous System Glia. Cold Spring Harb. Perspect. Biol. 7, a020552. 10.1101/cshperspect.a020552. [PubMed: 25722465]
49. Hakim-Mishnaevski K, Flint-Brodsly N, Shklyar B, Levy-Adam F, and Kurant E (2019). Glial Phagocytic Receptors Promote Neuronal Loss in Adult Drosophila Brain. Cell Rep. 29, 1438–1448. 10.1016/j.celrep.2019.09.086. [PubMed: 31693886]
50. Purice MD, Speese SD, and Logan MA (2016). Delayed glial clearance of degenerating axons in aged Drosophila is due to reduced PI3K/Draper activity. Nat. Commun. 7, 12871. 10.1038/ncomms12871. [PubMed: 27647497]
51. MacDonald JM, Beach MG, Porpiglia E, Sheehan AE, Watts RJ, and Freeman MR (2006). The Drosophila cell corpse engulfment receptor Draper mediates glial clearance of severed axons. Neuron 50, 869–881. 10.1016/j.neuron.2006.04.028. [PubMed: 16772169]
52. Musashe DT, Purice MD, Speese SD, Doherty J, and Logan MA (2016). Insulin-like Signaling Promotes Glial Phagocytic Clearance of Degenerating Axons through Regulation of Draper. Cell Rep. 16, 1838–1850. 10.1016/j.celrep.2016.07.022. [PubMed: 27498858]

53. Ray A, Speese SD, and Logan MA (2017). Glial Draper Rescues Abeta Toxicity in a Drosophila Model of Alzheimer's Disease. J. Neurosci. 37, 11881–11893. 10.1523/JNEUROSCI.0862-17.2017. [PubMed: 29109235]
54. Lee CYD, and Landreth GE (2010). The role of microglia in amyloid clearance from the AD brain. J. Neural Transm. 117, 949–960. 10.1007/s00702-010-0433-4. [PubMed: 20552234]
55. Alassaf M, and Rajan A (2023). Diet-induced glial insulin resistance impairs the clearance of neuronal debris in Drosophila brain. PLoS Biol. 21, e3002359. 10.1371/journal.pbio.3002359. [PubMed: 37934726]
56. Droujinine IA, and Perrimon N (2016). Interorgan Communication Pathways in Physiology: Focus on Drosophila. Annu. Rev. Genet. 50, 539–570. 10.1146/annurev-genet-121415-122024. [PubMed: 27732790]
57. Rajan A, and Perrimon N (2012). Drosophila cytokine unpaired 2 regulates physiological homeostasis by remotely controlling insulin secretion. Cell 151, 123–137. 10.1016/j.cell.2012.08.019. [PubMed: 23021220]
58. Freeman MR, and Doherty J (2006). Glial cell biology in Drosophila and vertebrates. Trends Neurosci. 29, 82–90. 10.1016/j.tins.2005.12.002. [PubMed: 16377000]
59. Xu Y, Xue D, Bankhead A 3rd, and Neamati N (2020). Why All the Fuss about Oxidative Phosphorylation (OXPHOS)? J. Med. Chem. 63, 14276–14307. 10.1021/acs.jmedchem.0c01013. [PubMed: 33103432]
60. Lunt SY, and Vander Heiden MG (2011). Aerobic glycolysis: meeting the metabolic requirements of cell proliferation. Annu. Rev. Cell Dev. Biol. 27, 441–464. 10.1146/annurev-cellbio-092910-154237. [PubMed: 21985671]
61. Israelsen WJ, and Vander Heiden MG (2015). Pyruvate kinase: Function, regulation and role in cancer. Semin. Cell Dev. Biol. 43, 43–51. 10.1016/j.semcdb.2015.08.004. [PubMed: 26277545]
62. Rai M, Carter SM, Shefali SA, Chawla G, and Tennessen JM (2024). Characterization of genetic and molecular tools for studying the endogenous expression of Lactate dehydrogenase in Drosophila melanogaster. PLoS One 19, e0287865. 10.1371/journal.pone.0287865. [PubMed: 38170735]
63. Yao CH, Wang R, Wang Y, Kung CP, Weber JD, and Patti GJ (2019). Mitochondrial fusion supports increased oxidative phosphorylation during cell proliferation. Elife 8, e41351. 10.7554/eLife.41351. [PubMed: 30694178]
64. Mishra P, and Chan DC (2016). Metabolic regulation of mitochondrial dynamics. J. Cell Biol. 212, 379–387. 10.1083/jcb.201511036. [PubMed: 26858267]
65. Arce-Molina R, Cortes-Molina F, Sandoval PY, Galaz A, Alegria K, Schirmeier S, Barros LF, and San Martin A (2020). A highly responsive pyruvate sensor reveals pathway-regulatory role of the mitochondrial pyruvate carrier MPC. Elife 9, e53917. 10.7554/eLife.53917. [PubMed: 32142409]
66. Serra D, Mera P, Malandrino MI, Mir JF, and Herrero L (2013). Mitochondrial fatty acid oxidation in obesity. Antioxid. Redox Signal. 19, 269–284. 10.1089/ars.2012.4875. [PubMed: 22900819]
67. Chen IC, Awasthi D, Hsu CL, Song M, Chae CS, Dannenberg AJ, and Cubillos-Ruiz JR (2022). High-Fat Diet-Induced Obesity Alters Dendritic Cell Homeostasis by Enhancing Mitochondrial Fatty Acid Oxidation. J. Immunol. 209, 69–76. 10.4049/jimmunol.2100567. [PubMed: 35697385]
68. Chang JS (2023). Recent insights into the molecular mechanisms of simultaneous fatty acid oxidation and synthesis in brown adipocytes. Front. Endocrinol. 14, 1106544. 10.3389/fendo.2023.1106544.
69. Welte MA, Cermelli S, Griner J, Viera A, Guo Y, Kim DH, Gindhart JG, and Gross SP (2005). Regulation of lipid-droplet transport by the perilipin homolog LSD2. Curr. Biol. 15, 1266–1275. 10.1016/j.cub.2005.06.062. [PubMed: 16051169]
70. Gronke S, Beller M, Fellert S, Ramakrishnan H, Jackle H, and Kuhnlein RP (2003). Control of fat storage by a Drosophila PAT domain protein. Curr. Biol. 13, 603–606. [PubMed: 12676093]
71. Li S, Raza SHA, Zhao C, Cheng G, and Zan L (2020). Overexpression of PLIN1 Promotes Lipid Metabolism in Bovine Adipocytes. Animals. 10, 1944. 10.3390/ani10111944. [PubMed: 33105676]

72. Yang A, and Mottillo EP (2020). Adipocyte lipolysis: from molecular mechanisms of regulation to disease and therapeutics. Biochem. J. 477, 985–1008. 10.1042/BCJ20190468. [PubMed: 32168372]

73. Beller M, Bulankina AV, Hsiao HH, Urlaub H, Jäckle H, and Kühnlein RP (2010). PERILIPIN-dependent control of lipid droplet structure and fat storage in Drosophila. Cell Metab. 12, 521–532. 10.1016/j.cmet.2010.10.001. [PubMed: 21035762]

74. Tiwari SK, Toshniwal AG, Mandal S, and Mandal L (2020). Fatty acid beta-oxidation is required for the differentiation of larval hematopoietic progenitors in Drosophila. Elife 9, e53247. 10.7554/eLife.53247. [PubMed: 32530419]

75. Fan J, Lin R, Xia S, Chen D, Elf SE, Liu S, Pan Y, Xu H, Qian Z, Wang M, et al. (2016). Tetrameric Acetyl-CoA Acetyltransferase 1 Is Important for Tumor Growth. Mol. Cell 64, 859–874. 10.1016/j.molcel.2016.10.014. [PubMed: 27867011]

76. Baker SA, and Rutter J (2023). Metabolites as signalling molecules. Nat. Rev. Mol. Cell Biol. 24, 355–374. 10.1038/s41580-022-00572-w. [PubMed: 36635456]

77. Aguer C, McCoin CS, Knotts TA, Thrush AB, Ono-Moore K, McPherson R, Dent R, Hwang DH, Adams SH, and Harper ME (2015). Acylcarnitines: potential implications for skeletal muscle insulin resistance. FASEB J. 29, 336–345. 10.1096/fj.14-255901. [PubMed: 25342132]

78. Martinez-Reyes I, and Chandel NS (2020). Mitochondrial TCA cycle metabolites control physiology and disease. Nat. Commun. 11, 102. 10.1038/s41467-019-13668-3. [PubMed: 31900386]

79. Zheng DM, An ZN, Ge MH, Wei DZ, Jiang DW, Xing XJ, Shen XL, and Liu C (2021). Medium & long-chain acylcarnitine's relation to lipid metabolism as potential predictors for diabetic cardiomyopathy: a metabolomic study. Lipids Health Dis. 20, 151. 10.1186/s12944-021-01576-9. [PubMed: 34727932]

80. Gottlieb RA, and Stotland A (2015). MitoTimer: a novel protein for monitoring mitochondrial turnover in the heart. J. Mol. Med. 93, 271–278. 10.1007/s00109-014-1230-6. [PubMed: 25479961]

81. Laker RC, Xu P, Ryall KA, Sujkowski A, Kenwood BM, Chain KH, Zhang M, Royal MA, Hoehn KL, Driscoll M, et al. (2014). A novel MitoTimer reporter gene for mitochondrial content, structure, stress, and damage in vivo. J. Biol. Chem. 289, 12005–12015. 10.1074/jbc.M113.530527. [PubMed: 24644293]

82. Shimazu T, Hirschey MD, Newman J, He W, Shirakawa K, Le Moan N, Grueter CA, Lim H, Saunders LR, Stevens RD, et al. (2013). Suppression of oxidative stress by beta-hydroxybutyrate, an endogenous histone deacetylase inhibitor. Science 339, 211–214. 10.1126/science.1227166. [PubMed: 23223453]

83. Yang D, Wang X, Zhang L, Fang Y, Zheng Q, Liu X, Yu W, Chen S, Ying J, and Hua F (2022). Lipid metabolism and storage in neuroglia: role in brain development and neurodegenerative diseases. Cell Biosci. 12, 106. 10.1186/s13578-022-00828-0. [PubMed: 35831869]

84. Allen NJ, and Lyons DA (2018). Glia as architects of central nervous system formation and function. Science 362, 181–185. 10.1126/science.aat0473. [PubMed: 30309945]

85. Frost JL, and Schafer DP (2016). Microglia: Architects of the Developing Nervous System. Trends Cell Biol. 26, 587–597. 10.1016/j.tcb.2016.02.006. [PubMed: 27004698]

86. Freeman MR, Delrow J, Kim J, Johnson E, and Doe CQ (2003). Unwrapping glial biology: Gcm target genes regulating glial development, diversification, and function. Neuron 38, 567–580. 10.1016/s0896-6273(03)00289-7. [PubMed: 12765609]

87. Hoopfer ED, McLaughlin T, Watts RJ, Schuldiner O, O'Leary DDM, and Luo L (2006). Wlds protection distinguishes axon degeneration following injury from naturally occurring developmental pruning. Neuron 50, 883–895. 10.1016/j.neuron.2006.05.013. [PubMed: 16772170]

88. Awasaki T, Tatsumi R, Takahashi K, Arai K, Nakanishi Y, Ueda R, and Ito K (2006). Essential role of the apoptotic cell engulfment genes draper and ced-6 in programmed axon pruning during Drosophila metamorphosis. Neuron 50, 855–867. 10.1016/j.neuron.2006.04.027. [PubMed: 16772168]

89. Grönke S, Mildner A, Fellert S, Tennagels N, Petry S, Müller G, Jäckle H, and Kühnlein RP (2005). Brummer lipase is an evolutionary conserved fat storage regulator in Drosophila. Cell Metab. 1, 323–330. [PubMed: 16054079]

90. Gronke S, Muller G, Hirsch J, Fellert S, Andreou A, Haase T, Jackle H, and Kuhnlein RP (2007). Dual lipolytic control of body fat storage and mobilization in Drosophila. PLoS Biol. 5, e137. 10.1371/journal.pbio.0050137. [PubMed: 17488184]

91. Sellin J, Fülle JB, Thiele C, Bauer R, and Bülow MH (2020). Free fatty acid determination as a tool for modeling metabolic diseases in Drosophila. J. Insect Physiol. 126, 104090. 10.1016/j.jinsphys.2020.104090. [PubMed: 32730782]

92. Puchalska P, and Crawford PA (2017). Multi-dimensional Roles of Ketone Bodies in Fuel Metabolism, Signaling, and Therapeutics. Cell Metab. 25, 262–284. 10.1016/j.cmet.2016.12.022. [PubMed: 28178565]

93. Maalouf M, Rho JM, and Mattson MP (2009). The neuroprotective properties of calorie restriction, the ketogenic diet, and ketone bodies. Brain Res. Rev. 59, 293–315. 10.1016/j.brainresrev.2008.09.002. [PubMed: 18845187]

94. Cheng J, Zhang R, Xu Z, Ke Y, Sun R, Yang H, Zhang X, Zhen X, and Zheng LT (2021). Early glycolytic reprogramming controls microglial inflammatory activation. J. Neuroinflammation 18, 129. 10.1186/s12974-021-02187-y. [PubMed: 34107997]

95. Yang S, Qin C, Hu ZW, Zhou LQ, Yu HH, Chen M, Bosco DB, Wang W, Wu LJ, and Tian DS (2021). Microglia reprogram metabolic profiles for phenotype and function changes in central nervous system. Neurobiol. Dis. 152, 105290. 10.1016/j.nbd.2021.105290. [PubMed: 33556540]

96. Brent AE, and Rajan A (2020). Insulin and Leptin/Upd2 Exert Opposing Influences on Synapse Number in Fat-Sensing Neurons. Cell Metab. 32, 786–800. 10.1016/j.cmet.2020.08.017. [PubMed: 32976758]

97. Madan A, Kelly KP, Bahk P, Sullivan CE, Poling ME, Brent AE, Alassaf M, Dubrulle J, and Rajan A (2024). Atg8/LC3 controls systemic nutrient surplus signaling in flies and humans. Curr. Biol. 34, 3327–3341. 10.1016/j.cub.2024.06.005. [PubMed: 38955177]

98. Doherty J, Sheehan AE, Bradshaw R, Fox AN, Lu TY, and Freeman MR (2014). PI3K signaling and Stat92E converge to modulate glial responsiveness to axonal injury. PLoS Biol. 12, e1001985. 10.1371/journal.pbio.1001985. [PubMed: 25369313]

99. Hombria JC, Brown S, Hader S, and Zeidler MP (2005). Characterisation of Upd2, a Drosophila JAK/STAT pathway ligand. Dev. Biol. 288, 420–433. [PubMed: 16277982]

100. Sundaram VK, Schutza V, Schroter NH, Backhaus A, Bilsing A, Joneck L, Seelbach A, Mutschler C, Gomez-Sanchez JA, Schaffner E, et al. (2023). Adipo-glial signaling mediates metabolic adaptation in peripheral nerve regeneration. Cell Metab. 35, 2136–2152. 10.1016/j.cmet.2023.10.017. [PubMed: 37989315]

101. Flier JS (2019). Starvation in the Midst of Plenty: Reflections on the History and Biology of Insulin and Leptin. Endocr. Rev. 40, 1–16. 10.1210/er.2018-00179. [PubMed: 30357355]

102. Liu Z, Ding J, McMillen TS, Villet O, Tian R, and Shao D (2020). Enhancing fatty acid oxidation negatively regulates PPARs signaling in the heart. J. Mol. Cell. Cardiol. 146, 1–11. 10.1016/j.yjmcc.2020.06.008. [PubMed: 32592696]

103. Mann V, Sundaresan A, and Shishodia S (2024). Overnutrition and Lipotoxicity: Impaired Efferocytosis and Chronic Inflammation as Precursors to Multifaceted Disease Pathogenesis. Biology 13, 241. 10.3390/biology13040241. [PubMed: 38666853]

104. Crewe C, Funcke JB, Li S, Joffin N, Gliniak CM, Ghaben AL, An YA, Sadek HA, Gordillo R, Akgul Y, et al. (2021). Extracellular vesicle-based interorgan transport of mitochondria from energetically stressed adipocytes. Cell Metab. 33, 1853–1868. 10.1016/j.cmet.2021.08.002. [PubMed: 34418352]

105. Bailey AP, Koster G, Guillermier C, Hirst EMA, MacRae JI, Lechene CP, Postle AD, and Gould AP (2015). Antioxidant Role for Lipid Droplets in a Stem Cell Niche of Drosophila. Cell 163, 340–353. 10.1016/j.cell.2015.09.020. [PubMed: 26451484]

106. Liu L, Zhang K, Sandoval H, Yamamoto S, Jaiswal M, Sanz E, Li Z, Hui J, Graham BH, Quintana A, and Bellen HJ (2015). Glial lipid droplets and ROS induced by mitochondrial

defects promote neurodegeneration. Cell 160, 177–190. 10.1016/j.cell.2014.12.019. [PubMed: 25594180]

107. Thiam AR, and Dugail I (2019). Lipid droplet-membrane contact sites - from protein binding to function. J. Cell Sci. 132, jcs230169. 10.1242/jcs.230169. [PubMed: 31209063]
108. Su W, Chi Y, and An YA (2023). Editorial: Lipid droplets and mitochondria in metabolic diseases. Front. Physiol. 14, 1266356. 10.3389/fphys.2023.1266356. [PubMed: 37637148]
109. Yin J, Gibbs M, Long C, Rosenthal J, Kim HS, Kim A, Sheng C, Ding P, Javed U, and Yuan Q (2018). Transcriptional Regulation of Lipophorin Receptors Supports Neuronal Adaptation to Chronic Elevations of Activity. Cell Rep. 25, 1181–1192. 10.1016/j.celrep.2018.10.016. [PubMed: 30380410]
110. Tung TT, Nagaosa K, Fujita Y, Kita A, Mori H, Okada R, Nonaka S, and Nakanishi Y (2013). Phosphatidylserine recognition and induction of apoptotic cell clearance by Drosophila engulfment receptor Draper. J. Biochem. 153, 483–491. 10.1093/jb/mvt014. [PubMed: 23420848]
111. Hashimoto Y, Tabuchi Y, Sakurai K, Kutsuna M, Kurokawa K, Awasaki T, Sekimizu K, Nakanishi Y, and Shiratsuchi A (2009). Identification of lipoteichoic acid as a ligand for draper in the phagocytosis of Staphylococcus aureus by Drosophila hemocytes. J. Immunol. 183, 7451–7460. 10.4049/jimmunol.0901032. [PubMed: 19890048]
112. Kuraishi T, Nakagawa Y, Nagaosa K, Hashimoto Y, Ishimoto T, Moki T, Fujita Y, Nakayama H, Dohmae N, Shiratsuchi A, et al. (2009). Pretaporter, a Drosophila protein serving as a ligand for Draper in the phagocytosis of apoptotic cells. EMBO J. 28, 3868–3878. 10.1038/emboj.2009.343. [PubMed: 19927123]
113. Krejcova G, Morgantini C, Zemanova H, Lauschke VM, Kovarova J, Kubasek J, Nedbalova P, Kamps-Hughes N, Moos M, Aouadi M, et al. (2023). Macrophage-derived insulin antagonist ImpL2 induces lipoprotein mobilization upon bacterial infection. EMBO J. 42, e114086. 10.15252/embj.2023114086. [PubMed: 37807855]
114. Brent AE, and Rajan A (2020). Insulin and Leptin/Upd2 Exert Opposing Influences on Synapse Number in Fat-Sensing Neurons. Cell Metab. 32, 786–800. [PubMed: 32976758]
115. Mathias B, Anna VB, He-Hsuan H, Henning U, Herbert J, and Ronald PK (2010). PERILIPIN-dependent control of lipid droplet structure and fat storage in Drosophila. Cell. Metab. 12, 521–532. [PubMed: 21035762]
116. Lu TY, MacDonald JM, Neukomm LJ, Sheehan AE, Bradshaw R, Logan MA, and Freeman MR (2017). Axon degeneration induces glial responses through Draper-TRAF4-JNK signalling. Nat. Commun. 8, 14355. 10.1038/ncomms14355. [PubMed: 28165006]
117. Logan MA, Hackett R, Doherty J, Sheehan A, Speese SD, and Freeman MR (2012). Negative regulation of glial engulfment activity by Draper terminates glial responses to axon injury. Nat. Neurosci. 15, 722–730. 10.1038/nn.3066. [PubMed: 22426252]
118. Logan MA, and Speese SD (2020). In Vivo Analysis of Glial Immune Responses to Axon Degeneration in Drosophila melanogaster. Methods Mol. Biol. 2143, 321–338. 10.1007/978-1-0716-0585-1_24. [PubMed: 32524491]
119. Chaudhry A, Shi R, and Luciani DS (2020). A pipeline for multidimensional confocal analysis of mitochondrial morphology, function, and dynamics in pancreatic beta-cells. Am. J. Physiol. Endocrinol. Metab. 318, E87–E101. 10.1152/ajpendo.00457.2019. [PubMed: 31846372]
120. Hu Y, Comjean A, Rodiger J, Liu Y, Gao Y, Chung V, Zirin J, Perrimon N, and Mohr SE (2021). FlyRNAi.org-the database of the Drosophila RNAi screening center and transgenic RNAi project: 2021 update. Nucleic Acids Res. 49, D908–D915. 10.1093/nar/gkaa936. [PubMed: 33104800]
121. Kurup K, Matyi S, Giles CB, Wren JD, Jones K, Ericsson A, Raftery D, Wang L, Promislow D, Richardson A, and Unnikrishnan A (2021). Calorie restriction prevents age-related changes in the intestinal microbiota. Aging (Albany NY) 13, 6298–6329. 10.18632/aging.202753. [PubMed: 33744869]
122. Meador JP, Bettcher LF, Ellenberger MC, and Senn TD (2020). Metabolomic profiling for juvenile Chinook salmon exposed to contaminants of emerging concern. Sci. Total Environ. 747, 141097. 10.1016/j.scitotenv.2020.141097. [PubMed: 32781313]

123. Hanson AJ, Banks WA, Bettcher LF, Pepin R, Raftery D, and Craft S (2019). Cerebrospinal fluid lipidomics: effects of an intravenous triglyceride infusion and apoE status. Metabolomics 16, 6. 10.1007/s11306-019-1627-x. [PubMed: 31832778]

Highlights

- Obesogenic diet triggers a starvation-like metabolic response in adipose tissue
- Dysfunctional adipocyte mitochondrial and lipid metabolism impairs glial phagocytic function
- Adipocyte ApoB functions as a novel regulator of glial phagocytic competence
- LpR1, in ensheathing glia, is essential for proper glial response to axonal injury

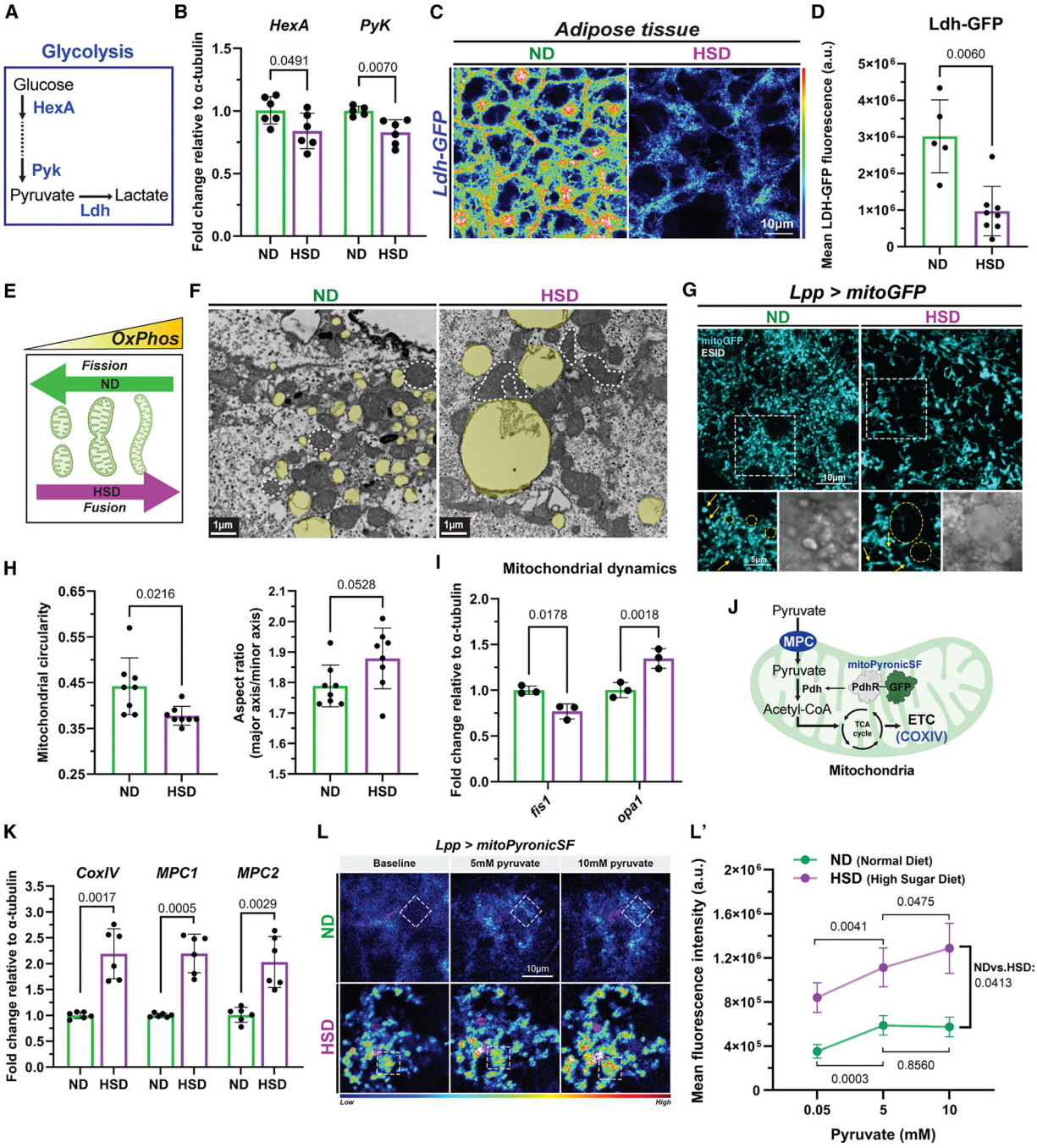

Figure 1. An HSD induces a metabolic shift in fly adipose tissue

(A) Schematic of glycolysis pathway enzymes (HexA, PyK, and Ldh).

(B and K) Fold change (qPCR) of the indicated mRNA relative to α-tubulin in the adipose tissue of flies fed either an ND or an HSD for 3 weeks. Student's t test with Welch's correction. $N = 3$ technical replicates of cDNA collected from 30 fly abdominal segments/treatment.

(C and D) Confocal images (C) and quantification (D) of adipocyte Ldh-GFP intensity. Scale bar: 10 μm. Student's t test (Welch's). Each dot represents an individual fly.

(E) Schematic: mitochondrial fission-fusion balance.
(F) TEM images of adipocyte mitochondria (white outline), ND vs. HSD at 1 week. Scale bar: 1 μm.
(G–I) Confocal mito-GFP images (G), mitochondrial circularity (H), and elongation (I). Scale bar: 10 μm (top) and 5 μm (bottom). Student's t test; dots represent individual flies.
(J) Mitochondrial pyruvate uptake.
(L and L′) Confocal live imaging (L) and quantification (L′) of mitochondrial pyruvate uptake (mitoPyronicSF) at baseline and pyruvate addition (5 and 10 mM). Scale bar: 10 μm. Student's t test.
All experiments except (F): 3 weeks of diet (ND or HSD). Statistical significance was determined using Student's t test (with Welch's correction where appropriate). Exact *p* values are indicated; all error bars represent ±SD. See also Figure S1.

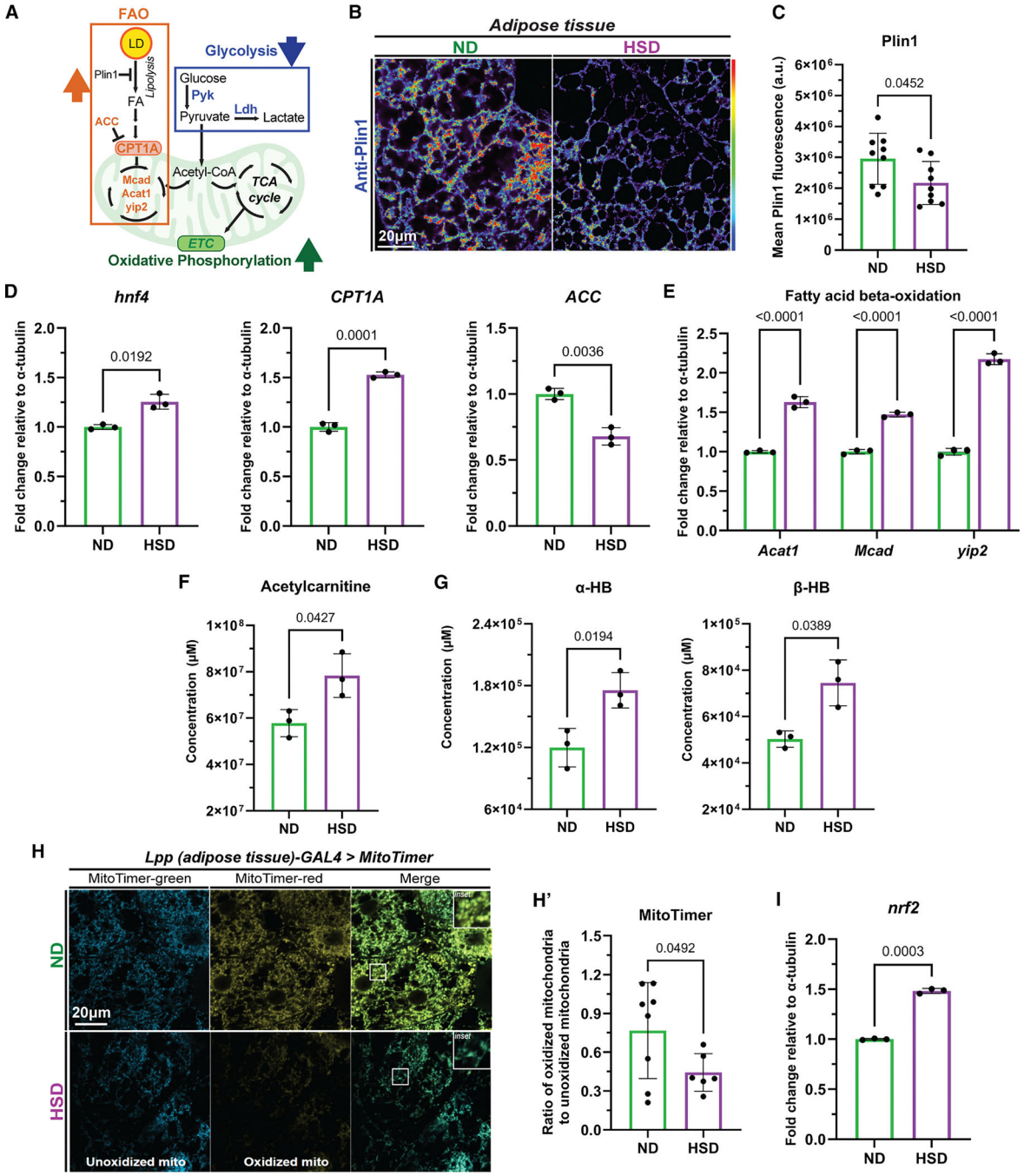

Figure 2. Molecular characterization of metabolic changes in the adipose tissue

(A) Schematic: metabolic shift toward FA oxidation (FAO) induced by an HSD.

(B and C) Confocal images (B) and quantification (C) of adipocyte Plin1 intensity in *w1118* fat bodies; ND vs. HSD. Scale bar: 20 µm. Student's t test (Welch's). Each dot represents an individual fly.

(D, E, and I) qPCR fold change of lipid metabolism (D), FAO enzyme genes (E), and antioxidant markers (I) in adult fat body explants; ND vs. HSD (3 weeks). Student's t test (Welch's) and one-way ANOVA; $N = 3$ replicates (each replicate contains 30 fat explants).

(F and G) Metabolite quantification (μM): acetylcarnitine, α-HB, and β-HB, in whole flies, ND vs. HSD (2 weeks). Student's t test (Welch's); $N = 3$ replicates. 10 flies per replicate. (H and H′) Confocal images (H) and quantification (H′) of mitochondrial oxidation (MitoTimer) in adipocytes. Scale bar: 20 μm.

Student's t test (Welch's); exact *p* values are indicated; dots represent individual flies; all error bars represent ±SD). See also Figure S2.

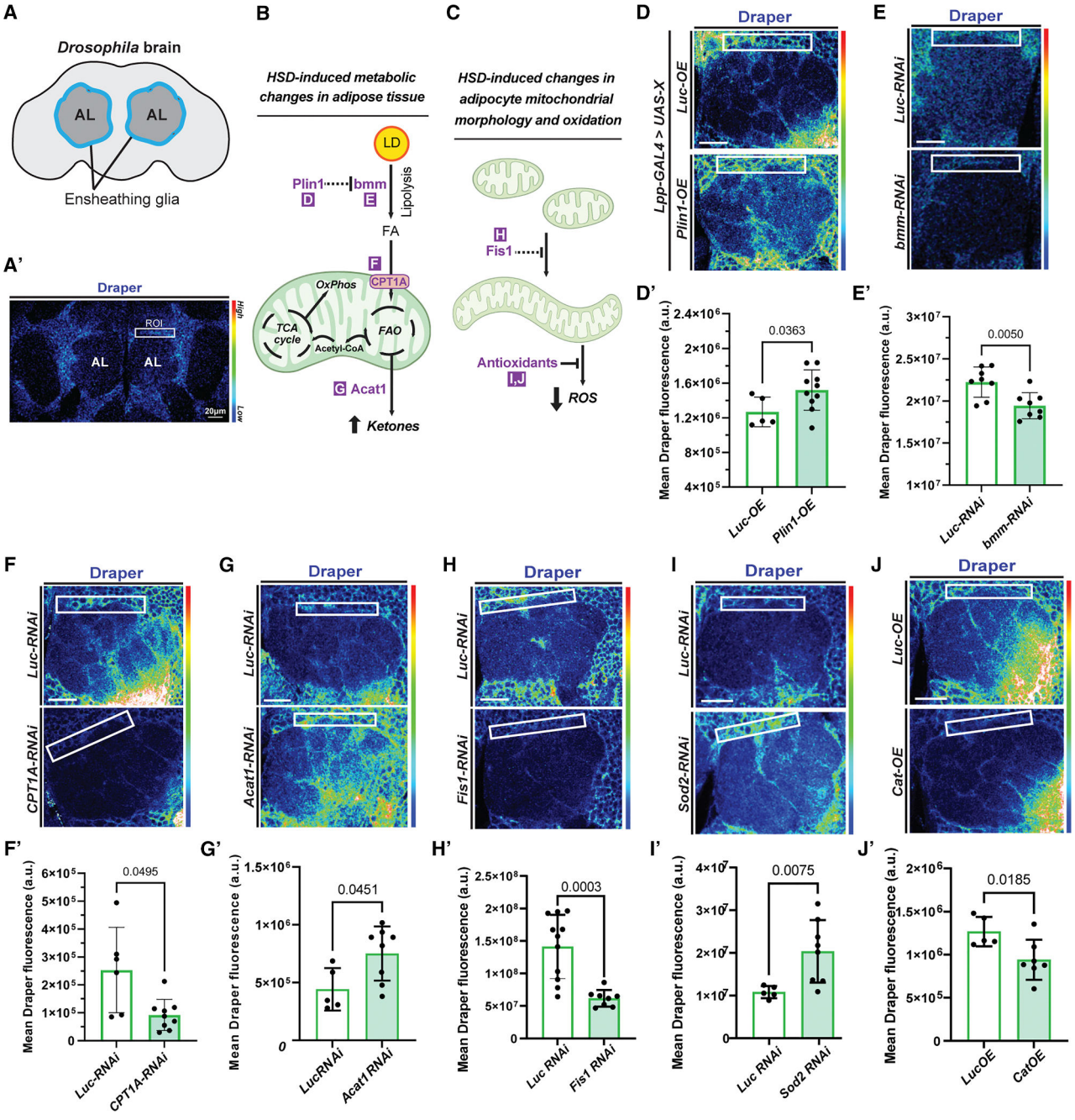

Figure 3. Adipocyte lipid metabolism and mitochondrial dynamics regulate Draper in ensheathing glia

(A–C) Schematics illustrating the experimental context.

(A) Adult fly brain schematic highlighting antennal lobes (ALs) and ensheathing glia.

(A′) Representative confocal image showing Draper staining in ALs; the inset defines the analyzed region of interest (ROI) in (D)–(J). Scale bar: 20 μm.

(B and C) Lipid metabolism and mitochondrial dynamics pathways, indicating adipocyte-specific genetic manipulations analyzed below.

(D–J) Representative confocal z stack projections showing Draper staining in ALs ensheathing glia from flies with adipocyte-specific gene knockdown (bottom) vs. matched controls (top). Scale bar: 20 μm.

(D′–J′) Quantification of Draper fluorescence intensity in ROIs (white boxes). Circles represent individual flies.

Student's t test with Welch's correction; exact *p* values are shown; all error bars represent ±SD. See also Figure S3.

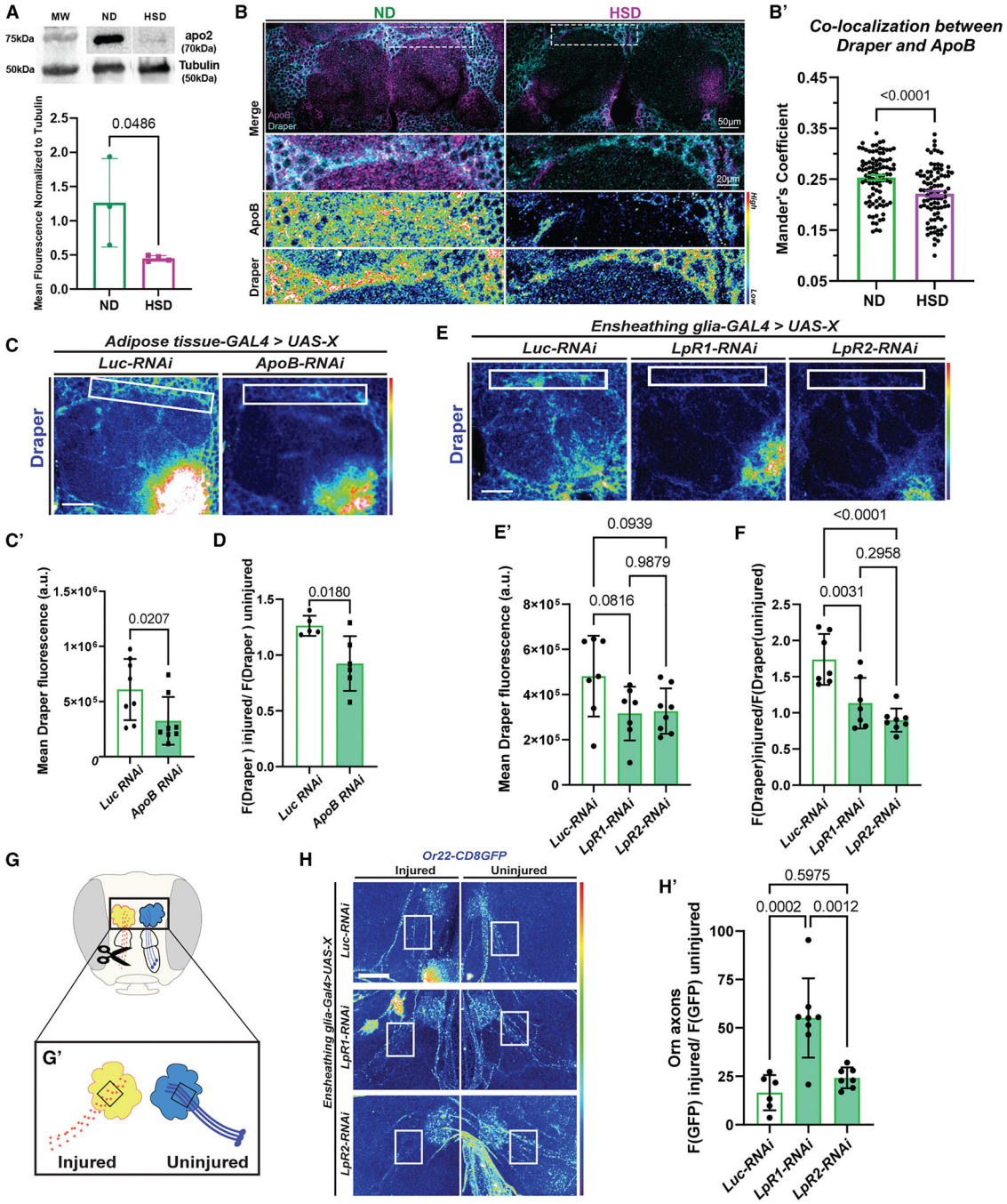

Figure 4. Adipocyte-derived ApoB modulates baseline glial phagocytic competence and injury response

(A and A′) Western blot (A) and quantification (A′) of brain ApoII levels in control (*w1118*) flies after 3 weeks of ND or HSD. ApoII was normalized to tubulin; dots represent 10 pooled brains each (3–4 replicates). Student's t test (Welch's correction); exact *p* value is shown.

(B and B′) Confocal images (B) and quantification (B′) of ApoB (purple) and Draper (cyan) co-localization (Manders' coefficient) in ALs from control flies (*w1118*, ND vs. HSD).

Insets show magnified merged and single-channel views. Dots represent single z-slices. Student's t test (Welch's); scale bars: 50 μm (top) and 20 μm (insets).

(C–F) Confocal z stacks are shown and quantificatied. Basal (C and E) and injury-induced (D and F) Draper staining in antennal lobes after adipocyte *ApoB-RNAi* or glial *LpR1-*, *LpR2-RNAi* vs. controls (*Luc-RNAi*).

(G–H′) Olfactory axon degeneration assay.

(G and G′) Schematic of unilateral antennal ablation in ORN22-CD8GFP flies.

(H and H′) Confocal z stacks (H) and quantification (H′) of GFP intensity in injured vs. uninjured axons after glial RNAi (*Luc*, *LpR1*, and *LpR2*), assessed 1 day post injury. Dots represent individual flies; Student's t test (Welch's); exact *p* values are shown; scale bar: 20 μm; all error bars represent ±SD. See also Figures S4–S6 and Tables S1 and S2.

KEY RESOURCES TABLE

REAGENT or RESOURCE	SOURCE	IDENTIFIER
Antibodies		
Chicken anti-GFP	Abcam	Cat#ab13970; RRID:AB_300798
Mouse anti-Draper	Developmental Studies Hybridoma Bank (DSHB)	RRID: AB_2618105 (clone 5D14)
Mouse anti-Draper	DSHB	RRID: AB_2618106 (clone 8A1)
Rabbit anti-Apo-II	Rajan Lab	Brent and Rajan[114]
Rabbit anti-Dilp5	Rajan Lab	Brent and Rajan[114]
Rabbit mito-mCherry	Abcam	Cat#ab167453, RRID: AB_2571870
Donkey anti-Chicken Alexa 488	Jackson ImmunoResearch	Cat#703-545-155; RRID: AB_2340375
Donkey anti-Rabbit Alexa 594	Jackson ImmunoResearch	Cat#711-585-152; RRID: AB_2340621
Donkey anti-Rabbit Alexa 488	Jackson ImmunoResearch	Cat#711-545-152; RRID: AB_2313584
Donkey anti-Mouse Alexa 594	Jackson ImmunoResearch	Cat#715-585-150; RRID: AB_2340854
Mouse anti-Tubulin	Sigma-Aldrich	Cat#T5168; RRID: AB_477579
Chemicals, peptides and recombinant proteins		
Pyruvate	Agilent	Cat#103578-100
HALT Protease Inhibitor Cocktail	ThermoFisher	Cat#87786
5x RIPA Buffer	ThermoFisher	Cat#J62524.AD
Laemmli Sample Buffer	Bio-Rad	Cat#161047
TCEP Bond Breaker	Thermo Scientific	Cat#77720
Precision Plus Protein™ Dual Color Standards	Bio-Rad	Cat#1610374
Starting Block™ Blocking Buffer	Thermo Scientific	Cat#37538
Enhanced Chemiluminescence (ECL) detection system	Abcam	Cat#AB65623
TriReagent	Sigma-Aldrich	Cat#T9424
iScript RT supermix	Bio-Rad	Cat#1708841
ssoAdvanced SYBR green master mix	Bio-Rad	Cat#1725270
Critical commercial assays		
Free Fatty Acid Assay Kit	Sigma-Aldrich	Cat#MAK466
Pierce™ BCA Protein Assay Kit	Thermo Scientific	Cat#23228
Direct-zol RNA microprep kit	Zymo Research	Cat#R2060
Deposited data		
Whole Fly Lysate Aqueous Metabolomic datasets for ND, HSD (7 and 14 days)	Figshare	https://doi.org/10.6084/m9.figshare.28765562.v1
Hemolymph Aqueous Metabolomic datasets for ND, HSD (7 and 14 days)	Figshare	https://doi.org/10.6084/m9.figshare.28765067.v2
Hemolymph Lipidomics datasets for ND, HSD (14 days)	Figshare	https://doi.org/10.6084/m9.figshare.28765064.v1
Experimental models: Organisms/strains		

REAGENT or RESOURCE	SOURCE	IDENTIFIER
UAS-Plin1:GFP	Kuhnlein Lab	Mathias[115]
Ldh-GFP	Tennessen Lab	Brent and Rajan[114]
ppl-Gal4	Leopold Lab	N/A
Lpp-Gal4	Eaton Lab	N/A
UAS-mitoTIMER	Bloomington *Drosophila* Stock Center (BDSC)	BDSC#57323
UAS-mitoPyronicSF	BDSC	BDSC#94536
UAS-Fis1-RNAi	BDSC	BDSC#63027
UAS-SOD2-RNAi	BDSC	BDSC#36871
UAS-Apolpp-RNAi	BDSC	BDSC#33388
UAS-LpR1-RNAi	BDSC	BDSC#27249
UAS-LpR2-RNAi	BDSC	BDSC#31150
UAS-Catalase	BDSC	BDSC#24621
UAS-whd-RNAi	BDSC	BDSC#34066
UAS-Acat1-RNAi	BDSC	BDSC#51785
Or22a-mCD8GFP	BDSC	BDSC#52620
Ensheathing glia-Gal4	BDSC	BDSC#39157
UAS-Luc-RNAi	BDSC	BDSC#31603
UAS-bmm-RNAi	Vienna *Drosophila* Resource Center (VDRC)	VDRC#37880
upd2-del	Zeidler Lab	N/A
Oligonucleotides		
Primers	See Table S3	See Table S3
Software and algorithms		
ImageJ	NIH	https://imagej.nih.gov/ij/
GraphPad PRISM	GraphPad Software Incorporated	https://www.graphpad.com/scientific-software/prism/
AB Sciex Analyst 1.6.3	AB Sciex	https://sciex.com/products/software/analyst-software
AB Sciex MultiQuant 3.0.3	AB Sciex	https://sciex.com/products/software/multiquant-software
Other		
Zeiss LSM 800 Confocal Microscope	Zeiss	N/A
Leica Stellaris Confocal Microscope	Leica Microsystems	N/A